



COMPASS
ENGINEERING LIFE GUIDED BY NATURE

This paper must be cited as: Bjørge, I. M., Correia, C. R., & Mano, J. Hipster microcarriers: exploring geometrical and topographical cues of non-spherical microcarriers in biomedical applications. Materials Horizons, (2022).

<https://doi.org/https://dx.doi.org/10.1039/d1mh01694f>

Hipster microcarriers: Exploring geometrical and topographical cues of non-spherical microcarriers in biomedical applications

Isabel M. Bjørge,^{a*} Clara R. Correia^{a*} and João F. Mano^{a*}

Structure and organisation are key aspects of the native tissue environment, which ultimately condition cell fate via a myriad of processes, including the activation of mechanotransduction pathways. By modulating the formation of integrin-mediated adhesions and consequently impacting cell contractility, engineered geometrical and topographical cues may be introduced to activate downstream signalling and ultimately control cell morphology, proliferation, and differentiation. Microcarriers appear as attractive vehicles for cell-based tissue engineering strategies aiming to modulate this 3D environment, but also as vehicles for cell-free applications, given the ease in tuning their chemical and physical properties. In this review, geometry and topography are highlighted as two preponderant features in actively regulating interactions between cells and the extracellular matrix. While most studies focus on the 2D environment, we focus on how the incorporation of these strategies in 3D systems could be beneficial. The techniques applied to design 3D microcarriers with unique geometries and surface topographical cues are covered, as well as specific tissue engineering approaches employing these microcarriers. In fact, successfully achieving a functional histoarchitecture may depend on a combination of fine-tuned geometrically shaped microcarriers presenting intricately tailored topographical cues. Lastly, we pinpoint microcarrier geometry as a key player in cell-free biomaterial-based strategies, and its impact on drug release kinetics, the production of steerable microcarriers to target tumour cells, and as protein or antibody biosensors.

Introduction

The cell microenvironment is a complex and hierarchical environment, where distinct cell populations interact and organise in specific architectures, in a tissue-dependent manner. Single cells give rise to functional subunits ranging anywhere between 100 µm and 1 mm that form the basis for each tissue.¹ Each cell is constantly exposed to biophysical and biochemical factors emerging from the direct and indirect contact with the extracellular matrix (ECM), neighbouring cells, soluble factors, and physical forces.² Although stable in the presence of minor perturbations, the cell phenotype is in fact pliable to external cues, which play a crucial role in regulating gene expression.¹ Within each tissue building block, ubiquitous physical cues guide cellular organisation and ultimately impact behaviour.² The capability of cells to translate the physical and mechanical cues delivered by the ECM into biochemical signals is a central aspect of how external cues modulate cellular functions and tissue organisation.³ At the nanometric scale, aligned collagen fibrils form the basic building block for both bone and tendon, where the key difference lies in the mineralised hydroxyapatite component of bone.⁴ Cardiomyocytes similarly align and elongate along fibrillar collagen and elastin bundles to form cardiac tissue.⁵ Geometry is a distinctive feature of hepatic lobules, characterised by their hexagonal form containing a central vein from which hepatic cords radiate, separated by vascular sinusoids.⁶ The distinctive design of each tissue highlights the importance of structural organisation in the native cell environment and point towards the advantage of applying physical cues and constraints to develop functional histoarchitectures.^{7,8}

From a tissue engineering perspective, biological factors such as growth factors remain the gold standard to induce cellular processes towards a functional regeneration. *In vitro*, biochemical factors can be easily introduced as a component of

the cell culture medium, yet the transposal to *in vivo* studies is more complex. With each targeted therapy, achieving a localised administration at an adequate concentration is still a necessary hurdle to overcome to reach the desired results in a clinical setting.⁹ An example is the controversy around the use of osteoinductive factor bone morphogenetic protein-2 (BMP-2) during spine fusion procedures, for which the FDA later issued a Public Health Notification due to life-threatening complications.¹⁰ The presentation of biophysical cues as opposed to biochemical signals has the advantage of bypassing such issues, while delivering similar outcomes. For instance, mesenchymal stromal cell differentiation can be guided towards distinct lineages simply by altering the physical/mechanical environment to which cells are exposed, such as tuning substrate stiffness¹¹ or introducing topographical features.¹²

It is well established that physical and mechanical aspects of a synthetically bioengineered ECM alter integrin-mediated cell adhesion and accordingly activate distinct downstream

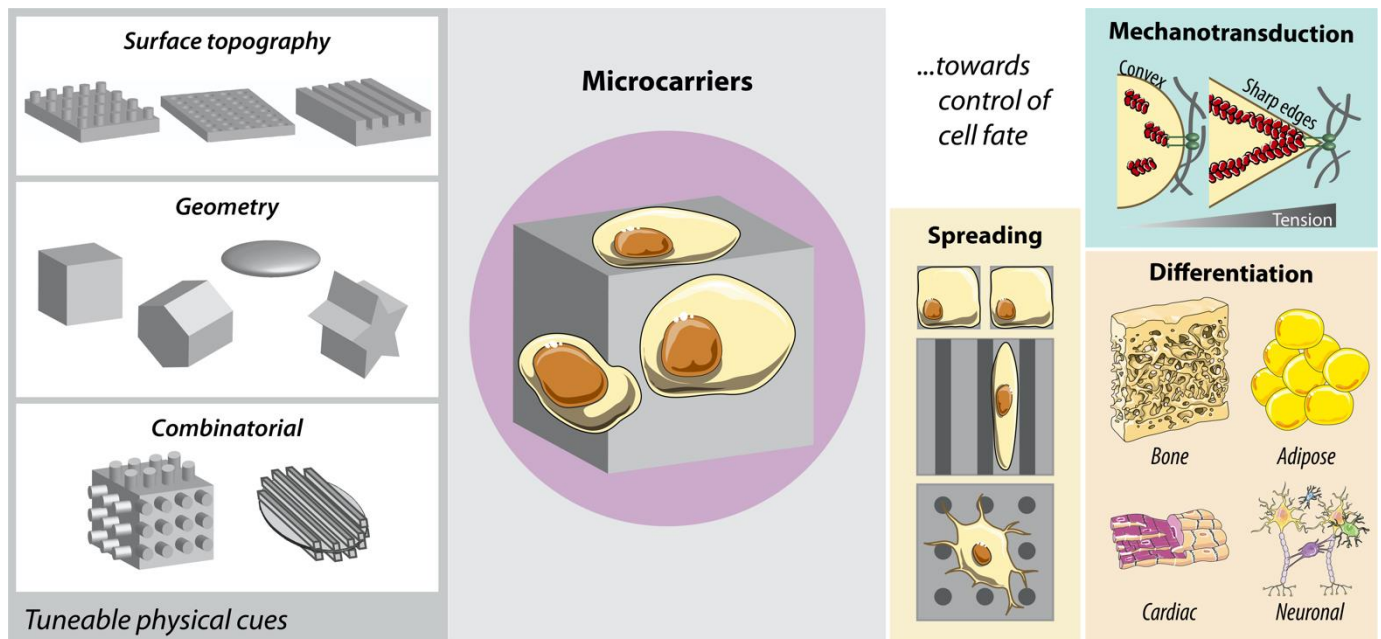


Figure 1. Microcarriers can be endowed with tuneable physical cues such as surface topography and geometry, or a combination of both, to modulate cell spreading and fate via mechanotransduction pathways to impact cell differentiation.

signalling pathways.^{13,14} As such, the role of surface cues on determining cell fate has been explored at the subcellular level using topographical features¹⁵ (grooves, pillars, and pits) and at a single cell or multicellular level via the application of geometrical features.¹⁶ These studies have elucidated the impacting and crucial role of both topographical and geometrical cues on the modulation of cell behaviour. However, these studies have been mainly performed in 2-dimensional (2D) environments, which fail to fully mimic the native cell environment. Options to take these studies into the third dimension rely mostly on bottom-up tissue engineering strategies using micrometric constructs, termed microcarriers. While microcarriers originally referred to spherical microparticles applied for adherent cell expansion in bioreactors, this term has since been broadened to range from cell-based tissue engineering approaches to drug delivery applications.

With this review, we aim to explore the current applications and advantages of non-spherical microcarriers, focusing on microcarriers with unique geometries and surface topographical features. Due to their modular, hierarchical context, we additionally include macroscale cell encapsulation approaches that rely on bottom-up assembly into larger constructs. While there are several recent research articles focusing on spherical microcarriers,^{17,18} and even microcarriers with distinct biochemical and biophysical cues,^{19,20} here we take a step further to delve deeper into the role of topography and geometry in directing cell fate, while addressing the mechanotransduction pathways inherently involved in this regulation and the impact of their transposal to the 3D context. To this end, relevant 2D studies are included that address the impact of cell-substrate interactions at the cellular level and mechanotransduction of geometrical/topographical cues to complement what is known, since the inclusion of such cues in

a 3-dimensional (3D) setting is an emerging field. Numerous techniques can be employed to design and produce these vehicles, as will be described further along in this review (Figure 1). We will also report the 3D applications and outcomes of advanced microcarriers opposing the classical spherical systems, which are recently being employed in TE, drug delivery, cell targeting, and biosensors. A special focus will be given to the role of geometrical and topographical cues not only in a 2D setting, as they are commonly applied, but the importance of transposing these cues into a 3D context, particularly for regenerative medicine applications.

Impact of cell-ECM interactions at the cellular level

In the native tissue environment, exchanges of biochemical and biophysical cues between neighbouring cells and cells from distinct lineages are mediated via interaction with the ECM.²¹ In a process termed mechanotransduction, physical and mechanical cues from the ECM are translated into biochemical signals.³ In general terms, most cell-ECM adhesions can be simplified into two major components, namely (i) transmembrane proteins, such as integrins that bind to the ECM or cadherins that bind to neighbouring cells, and (ii) actin fibres, which bind indirectly to transmembrane proteins via adaptor proteins.^{22,23} Upon integrin-mediated cell adhesion to the ECM, mechanical loading is exerted on adhesion sites with consequent force transmission.²¹ Force acts as a key regulator of the stability and lifetime of ligand-bound integrins and can lead to eventual bond dissociation for certain types of bonds²². Via force-induction, protein conformational changes or enzymatic reactions occur, which in turn direct biochemical signalling via integrin clustering and downstream signalling of integrin-mediated events. These include focal adhesion kinase

(FAK) activation or recruitment of adaptor proteins such as vinculin.^{21,22}

The molecular clutch controls tissue remodelling by regulating the transmission of force and cell migration.²³ The molecular clutch model considers that myosin contractility continuously powers actin flow towards the centre of the cell, termed retrograde flow.^{24,25} Upon integrin-based adhesion to the ECM, the elastic resistance to deformation offered by the ECM counters myosin contractility, which in turn slows down the actin retrograde flow (Figure 2). This however increases the force loading rate on the integrin-based adhesion complex.^{14,23} Depending on the type of bond behaviour for a given protein-protein interaction, the increased force loading rate can lead to either bond lifetime shortening or prolongation, for slip bonds and catch bonds, respectively.^{21,26} For example, rigid substrates induce higher loading rates, which in turn direct the unfolding of force-sensitive protein talin via catch bond formation, and consequent vinculin recruitment, decreased actin flow, growth of adhesion sites, and downstream signalling. Conversely, soft substrates with lower loading rates promote integrin detachment from the ECM prior to talin unfolding and bond reinforcement with vinculin.^{13,21} Due to this fact, whereas for cells adhered to rigid substrates the disruption of multiple actin stress fibres via laser nanoscissor severing only minimally disrupts cell morphology, a single fibre disruption for cells on soft substrates may greatly alter cell behaviour.²⁷ The molecular clutch model has also been demonstrated to govern cell sensing of substrate viscosity, with higher viscosity increasing loading rates and consequent talin unfolding and downstream signalling, which does not occur for lower viscosity. Lower matrix viscosity has also been linked to a rounded cell morphology due to an increasing ligand mobility and resulting reduction in cytoskeletal tension.¹⁴ Varying substrate coating density also impacts the rigidity threshold required for downstream signalling. For example, a reduction in coating density (e.g., with fibronectin) will decrease the number of available clutches. With actomyosin contractility distributed among fewer clutches, the loading force per clutch will increase accordingly, thus inducing talin unfolding and reinforcement at a lower rigidity threshold.¹³

Cells' capability to generate tension is thus impacted by the mechanical properties of the ECM, which in turn influences cell spreading, nuclear shape, activation of intercellular signalling pathways, and modulation of gene expression and transcription factors.^{28,29} Focal adhesions (FAs) are dynamic multiprotein complexes governed by external cues and cellular responses.³⁰ These may include integrins, as well as cytoskeletal and signalling proteins, such as talin, actinin, vinculin, zyxin, paxillin, and focal adhesion kinase (FAK).³¹ Furthermore, it has been suggested that cell adhesion in a 3D context may in fact differ from 2D focal and fibrillar adhesions in both molecular composition and localisation. FAs are mainly composed of separately localised $\alpha_v\beta_3$, paxillin, vinculin, and FAK, whereas fibrillar adhesions mostly contain $\alpha_5\beta_1$ integrin and tensin. Whereas tyrosine-phosphorylated FAK and paxillin are present in focal adhesions, a distinct trend is observed in fibrillar and 3D adhesions. Fibroblasts seeded in a 3D environment presented

triple co-localisation of α_5 integrin, paxillin, and fibronectin, with $\alpha_5\beta_1$ integrin playing a critical role. Additionally, even though 3D matrix adhesions present co-localisation of α_5 integrin with paxillin and FAK, as well as α_5 integrin co-localised with tyrosine-phosphorylated paxillin, the presence of tyrosine-phosphorylated FAK is only punctually observed, indicating another key difference between 2D and 3D adhesions.³²

Upon initial integrin-mediated adhesion, the increased local tension induces integrin clustering and phosphorylation of FAK. This activates small guanosine triphosphate hydrolases (GTPases) of the Rho-family such as RhoA, which in association with effector RhoA kinase (ROCK), phosphorylates myosin light-chain II (MLC). Subsequently, MLC binds and enhances non muscle myosin II heavy-chain activity, inducing actomyosin contractility.³³ Actomyosin contractility increases tension within the cytoskeleton with consequent enlargement and maturation of focal adhesion (FA) complexes and an ensuing greater traction on the ECM.^{28,34} Increasing matrix rigidity leads to upregulated myosin II contraction, which recruits and activates FAK.³⁵ Actin polymerisation, protease activation or secretion, and assembly/disassembly of focal contacts are regulated by FAK activity and downstream signalling.³⁰ Whereas Rho activation leads to the formation of FAs and may also activate FAK, a regulatory circuit exists where FAK in turn induces Rho down-regulation to prevent the formation of excessive adhesions. FAK-mediated Rho inhibition is hence required for FA turnover and cell migration.³¹ This is performed via direct interaction or phosphorylation of Rho GTPase protein activators or inhibitors.³⁰ FAK activation has also been linked to the activation of intracellular signalling cascades such as extracellular signal-regulated kinase–mitogen-activated protein kinase (ERK–MAPK) pathway, which impacts cell migration and proliferation.^{36,37} Aside from responding to ECM mechanical properties, cells may also induce ECM stiffening, hence directing matrix-mediated intercellular mechanical communication and collective durotaxis.³⁸

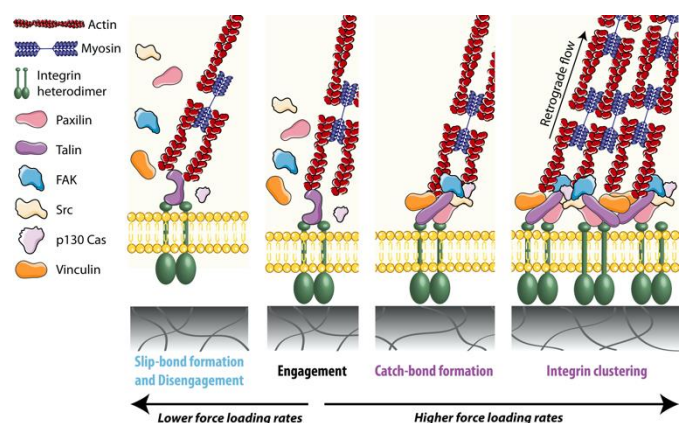


Figure 2. Molecular clutch model: upon integrin-mediated adhesion to the ECM, the increase in force loading rate on the integrin-based adhesion complex may direct the unfolding of force-sensitive protein talin via catch bond formation, and consequent vinculin recruitment, decreased actin flow, growth of adhesion sites, and downstream signalling. Impacting factors to integrin-mediated adhesions. Conversely, lower force loading rates lead to slip-bond formation and disengagement from the substrate. Integrin-mediated adhesions are impacted by substrate rigidity, ligand concentration, viscoelasticity, stress relaxation, topographical, and geometrical cues.

Cell spreading and migration

Cell spreading is similarly controlled by FA response to force and downstream regulation of Rho-family GTPases.³⁷ Changes in cell shape and cytoskeletal tension brought upon by cell adhesion are required for the activation of ROCK. Modulation via cell culture density or micro-island size can both impact cytoskeletal tension and consequently alter RhoA and ROCK expression.³⁹ Rho-family GTPases are involved in cell motility, adhesion, and cytoskeletal dynamics.¹⁵ They are also involved in the initiation of actin polymerisation and actin assembly with consequent formation of protrusions, in association with paxillin as a major regulator of protrusion growth. The formation of stress fibres, lamellipodia, and filopodia is directed by RhoA, Rac, and Cdc42 (cell division cycle 42), respectively.^{30,37} Cell spreading also impacts cell proliferation and appears as a requirement for anchorage-dependent cells to enter the S phase of the cell cycle.⁴⁰

Whereas cell migration on 2D substrates and nonlinearly elastic 3D environments is governed by the protrusion of lamellipodia, migration in a linearly elastic 3D structure, mimetic of the native cell environment, appears to occur via the extension of lobopodia. The formation and maintenance of lobopodia requires actomyosin contractility. In conjunction with nucleoskeleton-intermediate filament linker protein nesprin-3, a high cytoplasmic hydrostatic pressure in front of the nucleus is generated that drives the lobopodial membrane forward.⁴¹ In fact, migration in a 3D environment has been proposed to be similar to migration in a 1D environment, such as the one simulated by single fibres, as opposed to migration in 2D. Specifically, fibroblast migration on 1D fibrillar lines has been shown to be independent of ECM ligand density, but dependent on myosin II contractility and microtubules, similarly to cell migration within a 3D fibrillar cell-derived matrix. Whereas in 2D inhibition of contractility increases cell migration speed, speed in 1D and 3D is markedly hampered. Furthermore, fibroblasts in 1D demonstrate rapid spreading, polarisation, motility, and uniaxial phenotype, as would be expected in 3D.⁴² Moreover, hydrogel stress relaxation affects the spreading and proliferation of encapsulated fibroblasts, which are both increased with faster stress relaxation rates.⁴³

ECM mechanics as an impacting factor

In response to ECM mechanics, Rho GTPase activity and actomyosin tension induce YAP (Yes-associated protein) and TAZ (transcriptional coactivator with PDZ-binding motif or WWTR1) shuttling to the nucleus, which play a role in ECM remodelling.^{3,44} YAP/TAZ act as regulators of cell spreading and proliferation, shuttling from the cytoplasm to the nucleus in response to a soft or stiff environment, respectively.⁴⁵ Furthermore, YAP transcriptionally controls the formation of FAs and hence the degree of cell adhesion with consequent impact over cytoskeleton stability.⁴⁴ A study culturing MSCs on fibronectin-coated micropillars pinpointed nuclear localisation of YAP/TAZ as being primarily regulated by cell spreading/area and not cell-ECM contact area. Furthermore, rigid micropillars resulted in nuclear YAP/TAZ whereas elastic micropillars led to

cytoplasmic localisation.³ Another study using surface micropatterning for single-cell analysis, determined that a reduction in contact area led to a decrease in the number of FAs and a lower nuclear to cytoplasmic YAP localisation. However, for a constant cell spreading/area with decreasing contact area and consequent decrease in FAs, YAP nuclear localisation was not affected. This implies that cell area is in fact more crucial for YAP nuclear accumulation than the number of FAs formed during adhesion to the ECM.⁴⁴ In a 2D versus 3D encapsulation study of YAP/TAZ nuclear translocation in environments with identical substrate chemistry and varying stiffness, cell spreading was enhanced on stiffer 2D substrates, while softer substrates proved to enhance spreading within a 3D matrix. Correlating with YAP/TAZ relative nuclear intensity, increased nuclear localisation was observed for rigid substrates in 2D, while in 3D this was observed for softer and medium stiff hydrogels. When comparing MSCs seeded within same stiffness degradable or non-degradable hydrogels, it was demonstrated that cells acquired a more rounded morphology and presented a lower nuclear YAP/TAZ for non-degradable hydrogels. Hence, this highlighted the role of degradation on YAP/TAZ localisation, independently of hydrogel stiffness.⁴⁶

Notably, substrate rigidity has been linked to lineage-specific differentiation of MSCs, with soft gels (0.1-1 kPa) predominantly directing neurogenesis, while intermediately stiff gels (11 kPa) lead to myogenesis, and stiff gels (34 kPa) primarily induce osteogenesis. These stiffness-driven results were demonstrated to be linked with non-muscle myosin II expression.¹¹ Furthermore, the role of substrate stiffness on MSC osteogenic differentiation has been associated with the downstream up-regulation of specific proteins such as RhoA, YAP, and TAZ.¹⁴ Nuclear lamin-A overexpression has also been found to impact YAP1 nuclear localisation, indicating lamin-A as a modulator of several transcription pathways. Lamin-A expression has been implied as mechanosensitive, with high lamin-A concentrations stabilising the nucleus against stress on stiff surfaces. Furthermore, lamin-A knockout on soft substrates directed MSC differentiation into the adipogenic lineage, whereas overexpression on stiff substrates led to osteogenic differentiation.⁴⁷

Nevertheless, in 3D environments MSC commitment has been shown to occur even when cell and nuclear morphology were unaltered by substrate rigidity. Cell differentiation does still occur in response to mechanical stimulation, which regulates integrin binding and the reorganisation of adhesion ligands.⁴⁸ For instance, a similar cell morphology was observed between MSCs encapsulated within hydrogels with identical initial elastic modulus but with quite distinct stress relaxation rates, evidencing enhanced osteogenesis for faster stress relaxation. For slow-relaxing gels, an analogous trend in cell morphology was observed, with commitment to the adipogenic lineage ensuing with lower substrate elastic modulus, whereas osteogenesis occurred with higher elastic modulus. Generally, MSC commitment to the osteogenic lineage was observed in initially stiffer, faster relaxing hydrogels, while adipogenesis was promoted in initially softer hydrogels with slower stress relaxation. Faster relaxing viscoelastic matrices reportedly allow

for a greater matrix mechanical remodelling, which expedites adhesion-ligand clustering and adjustment of cell shape. ECM ligands were shown to mediate the effect of stress relaxation in the context of osteogenic differentiation, with an increased localisation of β_1 integrin at the cell periphery for faster relaxing gels. Furthermore, stiffer gels with faster stress relaxation presented an enhanced integrin clustering and greater actomyosin contractility, coincident with increased osteogenesis.⁴³ Yet, contrarily to previous studies stating the co-localisation of $\alpha_5\beta_1$ integrin, paxillin, and fibronectin in 3D matrix adhesions,^{32,49} paxillin was absent in the 3D environment for all levels of stress relaxation.⁴³ For both initial elastic moduli assessed, an increased YAP nuclear translocation was observed with faster stress relaxation. However, a similar nuclear to cytoplasmic YAP ratio was observed independently of elastic modulus, indicates that YAP localisation alone does not control MSC differentiation in 3D culture.⁴³ In both proteolytically degradable hydrogels as well as dynamic viscoelastic hydrogels, the enhancement of hMSC spreading, YAP/TAZ nuclear translocation, and osteogenic differentiation, has been shown to be mediated by cellular adhesion to nascent proteins. Upon inhibition of adhesion to nascent proteins or impaired remodelling, cell spreading was effectively reduced, which impacted downstream cellular outcomes such as YAP/TAZ nuclear translocation, and ultimately favoured commitment to the adipogenic lineage.⁴⁹

In fact, not only stromal cells are affected by the mechanical aspects of their environment. Morphology and function of hepatocytes have been shown to be impacted by substrate rigidity. Strikingly, increasing gel rigidity resulted in enhanced proliferation and dedifferentiation, whereas decreasing rigidity led to growth arrest and maintenance of phenotype.⁵⁰ When factoring in both rigidity and ligand concentration, a greater cell spreading was correlated with increased rigidity and ligand concentration. Conversely, albumin secretion, a downstream measure of hepatocyte function, followed the opposite trend with higher secretion rates for softer gels with lower ligand concentration, which was linked to decreased spreading.⁵¹ Interestingly, stiffness has also been pinpointed as a crucial factor in modulation of the immune response by leading to an altered function and phenotype of both immature and mature dendritic cells (DCs). Whereas substrate stiffness reportedly altered C-type lectin expression and consequently antigen internalisation in immature DCs, mature DCs presented altered CCR7 expression, which was linked to changes in migration towards chemokine CCL21 and a potentially hampered cell ability to reach lymph vessels.⁵²

Even though ECM mechanics have been the focus of several 2D and cell encapsulation studies, research on their impact for cell microcarriers is lacking. Considering current studies, it would be interesting to evaluate whether the same effects emerge in the more adaptable microcarrier environment. The same rationale applies to geometrical and topographical cues where, considering the impact of mechanical properties on the formation of FAs and consequent generation of tension by cells with corresponding onset of mechanotransduction events, it would be logical that such cues would also play a crucial role.

Curiously, in a 2D study, microtopography and stiffness showed an isolated but not combinatory impact on cell proliferation and differentiation.⁵³ It would be relevant to study further combinations of topography or geometry with stiffness or stress relaxation.

Mechanotransduction of topographical and geometrical cues in 2D and 3D contexts

A vast range of topographical cues have been explored in a 2D context. Topographical features such as pillars/columns,⁵⁴ pits,⁵⁵ roughness gradients,⁵⁶ localised curvature,⁵⁷ grooves,⁵⁸ and even random algorithm-generated topographies,^{59–61} condition cell morphology and impact cell behaviour. The most widely studied feature may in fact be nano- and microgrooves, which have been shown to direct the alignment of several types of cells, among which MSCs,⁵⁸ fibroblasts,⁶² cardiomyocytes,⁶³ osteoblasts,⁶⁴ and macrophages.⁶⁵ Similarly, geometrical features can restrict cell spreading and model cell morphology via the use of adhesive/non-adhesive spots to study the effects on single⁶⁶ or multiple⁶⁷ cells at a time. By tuning the size of adhesive spots, these can also be used to selectively target and modulate cell adhesion at the integrin-level,¹⁵ or model the cell as a whole.¹⁶ Hence, the question arises of which mechanotransduction pathways these topographical and geometrical cues trigger (Figure 3). Additionally, how this information may be leveraged and introduced to microcarrier-based approaches for 3D strategies.

Topographical cues

Given the micrometric breadth of integrin-based adhesions, cells are able to sense subcellular alterations in local ECM properties.⁶⁸ For instance, contact guidance of fibroblasts on grooved surface topography has been shown to be non-existent below features with a height of 35 nm,⁶⁹ yet an independent study demonstrated that fibroblasts can respond to nanopillars with a height as low as 8 nm.⁷⁰ Endothelial cells have been shown to spread substantially faster on grooved substrates than on flat substrates, particularly for groove depths below 1 μm (1 μm ridge/groove widths). Grooved topographical features accelerate initial cell spreading via integrin dependent FAK signalling, which in turn initiates downstream signalling for FA complex formation. Subsequently, contact guidance relies on ROCK and myosin II dependent cell contractility for maturation of FAs.⁷¹ The regulation of FA size is hence force-dependent and relies on actomyosin contractility.⁷² There are however contrasting reports on the effect of grooves on the size of FAs quantified using distinct parameters, such as area, width, or elongation. These differences may be attributed to varying groove dimensions such as groove/ridge width and depth, or even due to divergent responses of distinct cell populations. FA area was reportedly larger for endothelial cells seeded on grooves (1 μm ridge/groove/depth) than on flat substrates, yet by decreasing the depth to 800 nm these differences were abolished.⁷¹ Smaller and more elongated FAs were observed for hMSCs seeded on nanogrooves (250 nm) versus larger and less

elongated FA on microgrooves (10 μm) or flat substrates.⁷² Similarly, FA width of human corneal epithelial cells was highest for flat substrates and decreased in correspondence with decreasing ridge and groove widths, reaching a low for 70 nm ridges and 330 nm grooves.⁷³ Grooved (350 nm width) versus non-grooved substrates with distinct mechanical properties have illustrated the topography-dependent decrease in expression of integrin subunits α_1 , α_2 , α_6 , α_v , β_2 , β_3 and β_4 for the specific case of hMSCs cultured on grooves. This may indicate that differential integrins govern the transduction of grooved topographical cues to FA signalling components.⁷⁴ Initial contact also plays an important role in modulating cell behaviour. In quasi-3D sandwich cultures, cells were shown to maintain their morphology and spreading orientation even when stimulated with opposing physical cues to their dorsal region.⁷⁵ Interestingly, aside from the well documented induction of cell alignment by grooved surface topography, 12.5 μm wide grooves have also been shown to prompt the reorganisation of the nuclear lamina of fibroblasts, which provides structural support for the nucleus. Nuclear elongation in combination with cytoskeletal forces on the nucleus impact by repositioning chromosomal territories, primarily at the telomeric regions of the larger chromosomes. Transposing this to osteoblasts and considering that the major genes contributing to osteoblast functionality such as osteocalcin, osteopontin, Runx2, among others, are located within the telomeric regions of larger chromosomes, could explain a groove-induced facilitated accessibility to transcription factors.⁷⁶

Shallow nanoscale pits (14 and 29 nm) have been shown to increase spreading and cell attachment of human fetal osteoblastic cells (hFOB) when compared to deep pits (45 nm) or flat substrates. On shallower pits, hFOB integrin expression was demonstrated to be selective on specific integrin subunits, namely α_v , which has been linked to cell area and attachment. In combination with the presence of highly tensioned actin stress fibres anchored to paxillin, this points to an integrin α_v -paxillin-actin mediation of nanoscale topography. Changes in FAK autophosphorylation at tyrosine-397 on nanopits may also be linked to changes in integrin α_v and paxillin.⁷⁷ On columns (100 nm diameter), fibroblasts presented markedly fewer stress fibres and a rounded cell morphology, when compared with fibroblasts on flat surfaces. Interestingly, columns induced a slightly higher number of filopodia, which cells use to probe the surrounding environment.⁵⁴

Substrate curvature, convex or concave, has likewise been presented as an impacting factor on fibroblast behaviour. Fibroblasts cultured on top of glass spheres with diameters ranging from 5 μm to 2 mm embedded at the surface of hydrogels demonstrated that cell attachment rates and migration speeds declined as the sphere's diameter decreased. This was interrelated with a decrease in cell spreading, likely due to the increasing surface convexity inherent to smaller diameters.⁷⁸ The term "curvotaxis" has been attributed to the mechanism by which adherent cells react to curvature variations, specifically migrating towards negative curvatures. MSCs were shown to avoid convex regions during migration and

position themselves in concave regions, with the nucleus positioned at the most concave areas. Whereas short-lived and less-tensed FA were formed on convex curvatures, concave curvatures were marked by more stable FA due to the increased intracellular tension, contributing to preferential cell positioning in concave areas. Rho activity and its regulation of cell migration, actomyosin contractility, and FA is hence required for curvotaxis. Additionally, actin-dependent compression of the nucleus and consequent high lamin-A to stabilise the nucleus are required for curvature-induced nuclear movements and cell migration. Furthermore, curvotaxis requires LINC (Linkers of the Nucleoskeleton to the Cytoskeleton) complexes, given their role in enabling force transmission within the cell through the nucleus by bridging the nuclear lamina and cytoskeleton.⁵⁷ Correspondingly, actomyosin contractility was required for the alignment of endothelial cells and stress fibres on concave microgrooves (50 μm width). This effect was diminished upon treatment with blebbistatin, a myosin II inhibitor, which impacts cell contractility.⁷⁹

Interfacial roughness impacts mechanotransduction pathways and controls MSC adhesion and fate via FA formation, activation of signalling proteins, generation of nuclear tension, chromatin remodelling, and transcriptional activity. For roughness gradients ranging from 50 nm to 1.2 μm , cell spreading decreased and cell circularity increased with increasing substrate roughness. An intermediate interfacial roughness was associated with an increased adhesion due to an increased cellular contractility, evidenced via the formation of more pronounced actin stress fibres, paxillin localisation, and densest filopodia. Nuclear conformation was markedly impacted by distinct roughness gradients, reporting large smooth nuclei with higher lamin A/C intensity on low to intermediate roughness, versus small wrinkled nuclei with low lamin A/C for high roughness. Considering the impact of nuclear conformation and effects on chromatin remodelling and alteration of transcriptional activity, the differences stated may in fact play a role in the modulation of cell phenotype. Accordingly, YAP nuclear localisation peaked for intermediate roughness values. In mixed medium containing both osteoinductive and adipogenic factors, osteogenesis was favoured and adipogenesis suppressed. When solely containing osteoinductive or adipogenic factors, osteogenesis or adipogenesis were respectively induced, indicating the possible activation of distinct pathways.⁵⁶

In fact, it is well established that topographical cues do not only impact osteogenesis and adipogenesis via mechanotransduction. Accordingly, alignment and acquisition of an elongated morphology has been observed for human neural stem cells (hNSCs) cultured on substrates with nanogrooves alone (300 nm width with incremental spacing between features)⁸⁰ and on combination substrates with both microgrooves (1.5 μm width) with nanopits (10 nm diameter).⁸¹ When seeded on 300 nm diameter pillars with incremental spacing, cells became radially aligned.⁸⁰ With a 300 nm spacing between features, neuron differentiation was enhanced on nanogrooves comparatively to nanopillars, which was

correlated with an enhanced FA formation and upregulation of phosphorylated FAK. This was also observed when comparing substrates with a greater spacing between features. FAK phosphorylation in turn can activate downstream intracellular signalling of MEK-ERK pathways, which are involved in neurite outgrowth during stem cell differentiation.⁸⁰ Interestingly, hNSCs differentiation into functional neurons was enhanced on combination substrates featuring both microgrooves and nanopits when compared with flat substrates and substrates presenting only microgrooves or nanopits. These combination substrates presented an enhanced vinculin staining, as well as colocalization of integrin β_1 and neural cell adhesion molecule, even when compared with substrates presenting only a single feature. β_1 integrin-mediated binding in conjunction with ROCK-mediated intracellular signalling pathways promoted FA formation and FAK pathway activation, which enhanced differentiation of hNSCs. Furthermore, increased neurite sprouting from cell bodies was observed, which is known to augment cell-cell interactions and enhance hNSC differentiation via cell-cell signalling.⁸¹ ROCK downstream signalling has been associated with an increased actomyosin contractility. In particular, the up-regulated gene expression of neuronal markers in human embryonic stromal cells has been attributed to a higher actomyosin contractility on nanogrooves (250 nm).^{72,82} However, the expression level of microtubule-associated protein 2 (MAP2), a marker for mature neurons, was reduced via inhibition of myosin II, yet not by ROCK inhibition, indicating a ROCK-independent regulatory pathway of myosin II.⁸² Furthermore, the increased FAK phosphorylation and higher pFAK/FAK ratio on nanogrooved versus flat substrates was correlated with the increased MAP2 expression. The higher MAP2 expression was attributed to early FAK activation via topographical cues and not alterations in cell shape *per se*. A plausible explanation is that by regulating the spatial organisation and elongation of FA, grooves impact the pulling angle of actomyosin contractility within the cell.⁷²

For osteogenic differentiation, the selected cell population has been demonstrated to be an impacting factor with pre-osteoblastic cell line MC3T3-E1, hASCs, and periodontal ligament-derived stromal cells (PDLSCs) presenting commitment to the osteogenic lineage with distinct groove and ridge dimensions. Interestingly, the enhanced commitment to the osteogenic lineage for each cell type was linked with the maximum cell elongation, which may be linked to the tensile stress required for osteogenic differentiation.⁵⁸ On the micrometric scale with a fixed groove width of 5 μm , hMSCs cultured with supplements for specific lineage commitment, preferentially differentiated into the adipogenic lineage with increasing ridge width (15 μm), whereas decreasing ridge width (2 μm) preferentially induced osteogenesis. Interestingly, 600 nm wide grooves with 650 nm ridges directed both adipogenic and osteogenic differentiation of MSCs, yet no significant upregulation was observed in the absence of lineage commitment factors. Furthermore, YAP localisation remained unaffected on grooved versus flat substrates.⁸³ Another study featuring grooves (300 nm width) or pillars (450 nm diameter with hexagonal or square organisation) with surface

immobilised bone morphogenetic protein-2 (BMP-2) observed an increase in mineralisation and upregulation of osteogenic markers for these distinct topographical features as opposed to flat substrates. This result may in fact be linked to an augmented FA formation on substrates with topographical features, supported by an enhanced gene expression of FA assembly proteins such as vinculin and FAK.⁸⁴ Substrates with highly ordered topographical features have thus shown promising results in strategies aiming osteogenic differentiation. Interestingly, cell adhesion and osteogenic differentiation of osteoprogenitor cells was shown to be enhanced on nano-displaced pits (120 nm diameter pits, 100 nm deep), in contrast to a negligible effect observed for highly ordered nanotopographies.⁵⁵ Varying topographical cues have been shown to play a role in mineralisation, which could in fact be correlated with *in vivo* bone bonding to titanium implant.⁶⁰

Geometrical cues

While topographical features actively modulate cell morphology to some extent (e.g., cell alignment with grooves), they generally do not fully control single cell geometry. A practical approach to study the effects of 2D geometry on cell behaviour is via microcontact printing to create adhesive and non-adhesive regions. These regions can be tailored in size, biochemical composition and spatial localisation, and shape, from less to more complex geometries. Microcontact printing of linear cell adhesive fibronectin elements with varying line alignment, density, and width, demonstrated that cell alignment altered the number and location of protrusive edges initiated by active Rac1, and that a high alignment was correlated with a rapid directional cell migration.¹⁵ To assess the effects of anisotropic versus isotropic ligand arrangement on cytoskeletal organisation, circular and square geometries with distinct peripheral fibronectin localisation were patterned. An anisotropic ligand arrangement was shown to enhance actomyosin contractility and consequently redirected cell differentiation from adipogenic to osteogenic.⁶⁶

In endothelial cells, cell shape and spreading proved to be impacting factors in directing cell proliferation or apoptosis. Using multiple FA-sized islands versus islands accommodating an entire cell, an increased cell spreading with a constant cell-matrix contact area was enabled by further distancing FA-sized islands. Increasing cell spreading was correlated with an increased cell proliferation and abrogated apoptosis.¹⁶ While cell spreading is required for the formation of FAs and an increased spreading is correlated with a greater number of FAs, cytoskeletal tension has also been proven to play a role in moulding the shape and distribution of FAs and not integrin-ECM contact alone.⁸⁵ Also, by simply decreasing or increasing island size and hence the available surface area for cells to adhere, MSC fate could be directed to either adipogenic or osteogenic, respectively.⁸⁶ Cell shape reportedly modulated endogenous RhoA activity with osteogenic differentiation occurring only for spread cells with active RhoA, and adipogenic commitment requiring dominant-negative RhoA and unspread round cells. However, osteogenesis could be induced

independently of cell shape by directly inducing actomyosin contractility via ROCK activation.⁸⁷

Other major osteogenesis-promoting cues are cell aspect ratio and subcellular curvature. For example, commitment to the osteogenic lineage was boosted for single cells on rectangles (4:1 aspect ratio) versus squares (1:1). Concerning subcellular curvature, adipogenesis was favoured on flower shapes with large convex curves, while osteogenesis was preferentially induced on star-shapes with concave edges and sharp vertices. Star shapes reportedly induced larger FAs and stress fibres, with a consequent increase in actomyosin contractility and cytoskeletal tension. Actomyosin contractility stimulates MAPK cascades and Wnt signalling, via Wnt associated transcripts such as Rac1, Cdc42, RhoA, ROCK2, among others, which regulate differentiation into the osteogenic lineage. Geometries that led to lower contractility rendered cells more susceptible to adipogenic soluble factors, while downregulating Wnt signalling. Blocking selective cell surface integrin receptors also led to inhibition of osteogenesis due to the decreased tension exerted by the cell on the substrate. Furthermore, in the absence of lineage guidance soluble factors, stars expressed higher expression of GTPases involved in cell motility, Rac, and Cdc42, linked to greater polarity and protrusion.⁸⁶ Furthermore, high cell contractility has been shown to favour lipid raft formation, which triggers Akt recruitment to the plasma membrane and pathway activation towards osteogenic differentiation.⁸⁸

Convex features on 2D substrates were shown to promote the assembly of lamellipodia, whereas concave features led to the assembly of stress filaments, which was linked to changes in polarity of rat melanoma cells.⁸⁹ On non-adherent regions, specifically negative/concave curvatures, cell migration mediated by a combination of leading-edge actin cables and the local induction of a tension anisotropy gradient. Whereas protrusions on cell-sized positive/convex curvatures occurs via retrograde flow, on negative/concave curvatures actin cables were formed due to an anterograde flow towards the cell edge.⁹⁰ On T, Y, and U-shaped spots, cells initially acquired the shape of micropattern, and secondly generated contractile stress fibres to minimise the distance between apices. Accordingly, stronger contractile stress fibres spanned over non-adhesive edges than over adhesive edges.⁹¹ Aside from geometry, initial cell positioning is another preponderant factor for cell spreading, where corners require cell rotation and hence slow down cell spreading.⁹²

On multicellular islands, similar trends regarding low or high cellular tension and selective differentiation have been observed. Whereas osteogenic differentiation was induced at island edges, adipogenesis was stimulated at the centre, regardless of geometry (mixed osteogenic and adipogenic soluble factors). To isolate the effect of curvature, undulating geometries were assessed, and it was observed that cells on convex edges underwent osteogenic differentiation while concave edges directed adipogenesis. Cells on convex edges were subjected to forces in a magnitude three-fold higher than concave edges. Hence, high stress regions with increased actomyosin contractility were associated with osteogenic

differentiation, whereas low contractility on low stress regions induced adipogenesis. In a 3D microcarrier-based context, cells encapsulated within a collagen hydrogel also presented enhanced osteogenesis on the edge of constructs and adipogenesis in the core.⁶⁷ Particularly due to the effects of local curvature on cell fate, it would be interesting to explore the impact of microcarrier geometry upon implantation *in vivo*.

In a cell sheet model, a higher cell proliferation was localised in regions with enhanced tractional stress generated within the cell sheet. The geometry-dependent cell contraction originated patterns of mechanical stress which affected cell growth and highlighted the importance of tissue architecture.⁹³ Another approach using microfabricated tissue gauges (μ TUGs) allowed to produce collagen-embedded microtissues between a desired number of micropillars. Micropillars acted as anchoring points and allowed to control matrix alignment, measure microtissues' contractile forces and apply tensile strain. The mechanical stiffness of micropillars and collagen matrix impacted cellular contractile forces and matrix protein deposition, consequently altering tissue remodelling.⁹⁴ Pillar isotropic or anisotropic arrangement allowed to control matrix alignment between unaligned and aligned, respectively. Whereas higher microtissue stiffness was observed in aligned regions, this was not dependent on active cellular contractility, but was rather dictated by the collagen matrix and the cellular actin cytoskeletal network.⁹⁵

Taken together, these studies underline the relevance of both topographical and geometrical cues on the mediation and activation of mechanotransduction pathways, which subsequently govern multiple cellular actions, such as migration, proliferation, and differentiation, ultimately overseeing tissue composition and architecture. However, it is to note that a good degree of uncertainty and unpredictability still surround the influence of physical cues on cell behaviour. Furthermore, the question arises whether such physical cues are sensed only upon direct contact with the substrate or if cells indirectly transfer these cues to neighbouring cells. As the main adhesion proteins at intercellular junctions, cadherins also play their part in mechanosensing of fluctuations in actomyosin cytoskeletal tension and subsequent mechanotransduction.⁹⁶ It would be expected that such mechanisms would play a role in the indirect transmission of topographical and geometrical cues. With the evolution of biofabrication tools enabling an even tighter control over feature design, endless iterations of feature dimensions become possible. Combined with inherent

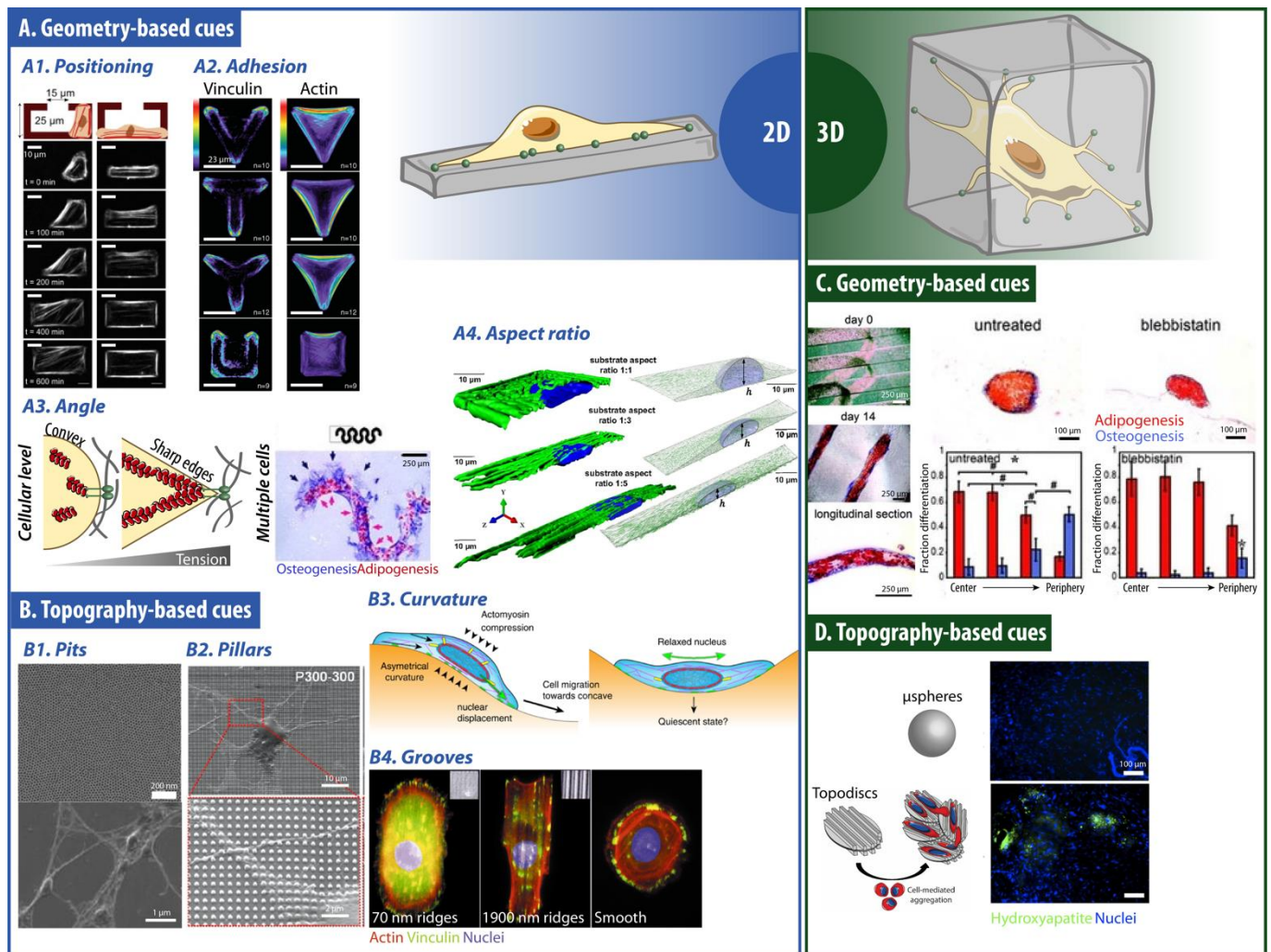


Figure 3. Geometrical and topographical cues applied in 2D and 3D to modulate cell behaviour. 2D – **A. Geometry-based cues:** Positioning (A1) [Reprinted with permission from ⁹², Copyright (2019) Elsevier]. Adhesion (A2) [Reprinted with permission from ⁹¹, Copyright (2006) John Wiley & Sons]. Angle (A3) [Reprinted with permission from ⁶⁷, Copyright (2009) John Wiley & Sons]. Aspect ratio (A4) [Reprinted with permission from ²⁵⁰, Copyright (2019) National Academy of Sciences]. **B. Topography-based cues:** Pits (B1) [Reprinted with permission from ⁸¹, Copyright (2014) American Chemical Society]. Pillars (B2) [Reprinted with permission from ⁸⁰, Copyright (2013) American Chemical Society]. Curvature (B3) [Reprinted with permission from ⁵⁷, Copyright (2018) Springer Nature]. Grooves (B4) [Reprinted with permission from ⁷³, Copyright (2003) Company of Biologists Ltd.]. 3D – **C. Geometry-based cues** [Reprinted with permission from ⁶⁷, Copyright (2009) John Wiley & Sons]. **D. Topography-based cues** [Reprinted with permission from ¹¹⁷, Copyright (2019) Royal Society of Chemistry].

differences for distinct cell populations, it becomes difficult to reach a universal consensus. High-throughput studies aim to bridge this gap by combining large scale screening with machine learning to rationally design biomaterial surfaces.^{59–61,97,98}

Microcarrier production methods

The application of microcarriers, particularly spherical microcarriers, in the regenerative medicine field is vast. Spherical microcarriers have been applied as vehicles for cell proliferation and expansion within bioreactors,⁹⁹ their biochemical surface properties have been tailored to enable the production of larger constructs via cell-mediated aggregation,¹⁰⁰ they have been utilised as cell encapsulation vehicles to direct localised *in vivo* tissue formation,¹⁰¹ among others. The scope of this review lies in exploring the applications and advantages of non-spherical microcarriers, focusing on

microcarriers with unique geometries and surface topographical features.

Non-spherical microparticles may be produced via distinct microfabrication techniques. For the production of spheroids and ellipsoids simpler techniques such as uniaxial stretching within sacrificial templates,^{102–108} emulsion-based,^{109–111} superhydrophobic surface-based,¹¹² and conventional continuous-flow microfluidic-based set-ups^{113,114} have been applied. To produce other standard geometric shapes, such as cylinders, rectangular, and triangular prisms, or even more complex geometries, alternative methods have been applied. Methods for production of these geometries include photolithography,¹¹⁵ and soft lithography techniques, such as replica moulding¹¹⁶ and imprinting¹¹⁷. Microfluidics-based strategies with continuous flow¹¹⁸ or stop-flow lithography,¹¹⁹ as well as optofluidics¹²⁰ are popular alternatives. Figure 4 highlights select examples for each of the fabrication methods

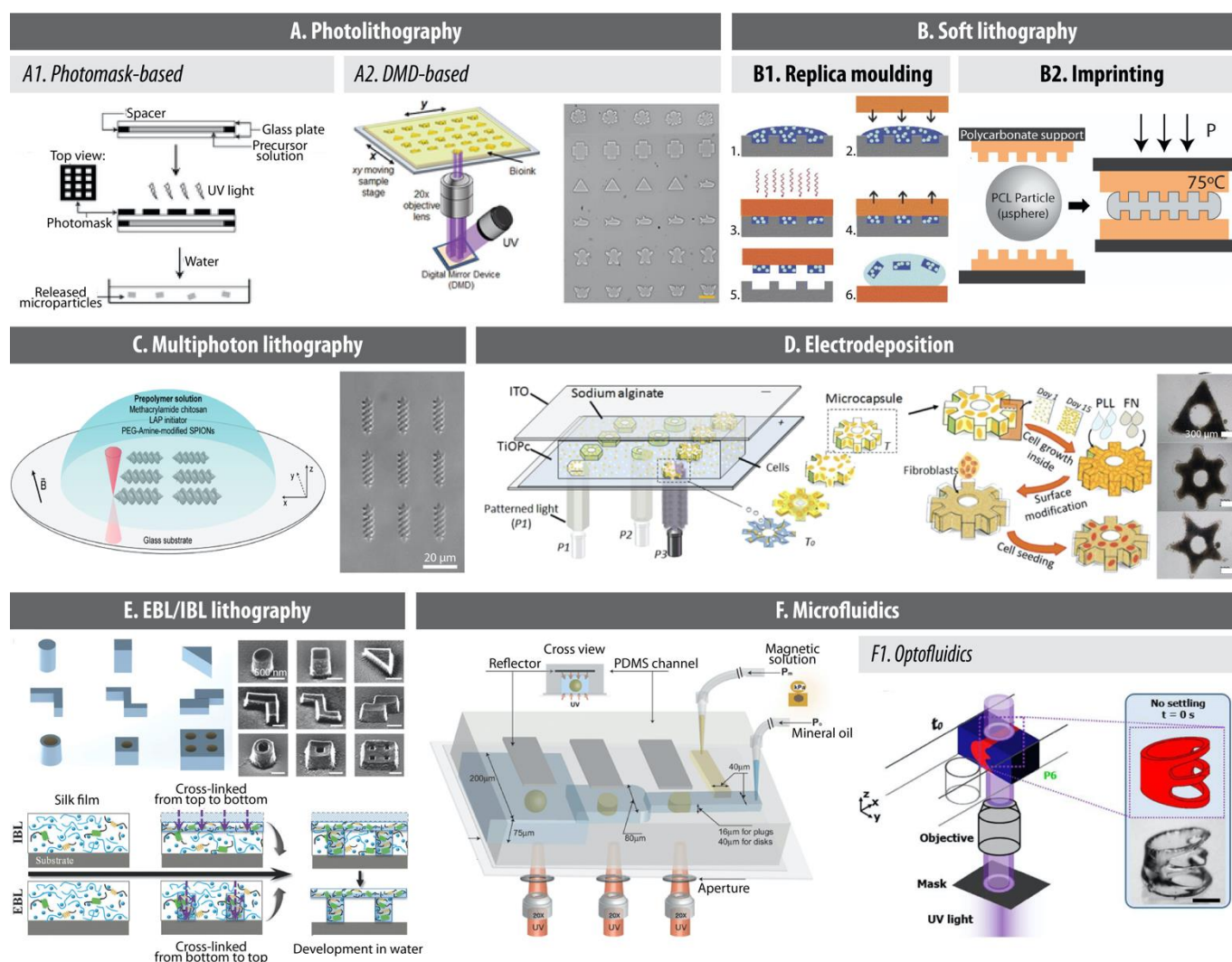


Figure 4. Microcarrier production methods. A. Photolithography: photomask-based (A1) and DMD-based (A2) [Reprinted with permission from ¹⁶⁷, Copyright (2007) American Chemical Society. Reprinted with permission from ¹⁶⁸, Copyright (2019) John Wiley & Sons]. B. Soft lithography: replica moulding (B1) and imprinting (B2) [Reprinted with permission from ¹²⁸, Copyright (2006) Elsevier. Reprinted with permission from ¹¹⁷, Copyright (2019) Royal Society of Chemistry]. C. Multiphoton lithography [Reprinted with permission from ¹⁷⁰, Copyright (2018) American Chemical Society]. D. Electrodeposition [Reprinted with permission from ¹⁴², Copyright (2019) American Chemical Society]. E. EBL/IBL lithography. [Reprinted with permission from ¹³⁸, Copyright (2018) John Wiley & Sons]. F. Microfluidics and optofluidics (F1) [Reprinted with permission from ¹⁸⁹, Copyright (2008) Royal Society of Chemistry. Reprinted with permission from ¹²⁰, Copyright (2016) Royal Society of Chemistry].

described in this section, namely photolithography (photomask-based and digital mirror device (DMD)-based), soft lithography (replica moulding and imprinting), multiphoton lithography, electrodeposition, electron beam and ion beam lithography (EBL and IBL), microfluidics, and optofluidics. Additionally, Table 1 summarises the methods and respective materials used to produce microcarriers with variable geometries and topographical cues.

Photolithography

Photolithography relies on a projection-printing system where relief patterns are created via the projection of radiation within or near the UV-visible section of the electromagnetic spectrum. The technology uses an illumination system composed of a source and condenser lens assembly, as well as a photomask for region selective projection. The main limitation of

photolithography hinges on the resolution, which is approximately half the wavelength of the illuminating light and is governed not only by the illuminating light but also the aperture of the projection lens. Initially dependent on visible g-line (436 nm) and UV i-line (365 nm) sources, current technologies may resort to extreme-UV light (13.5 nm), which greatly increases resolution.^{121,122} To produce hydrogel-based microcarriers, and in particular microcarriers aiming towards cell encapsulation, photolithography is an attractive and widely applied technique. Cells can be uniformly dispersed throughout the construct, and the control over spatial and temporal reaction kinetics can be easily achieved. However, both UV exposure time and photoinitiator concentration should be taken into consideration as they impact cell viability due to the generation of cytotoxic free radicals.¹²³ Nonetheless, taking advantage of current biotechnology solutions, these issues can be easily minimised and interesting applications developed. For

instance, fibroblast-encapsulating PEGDA-based microunits were produced via photolithography and further assembled into larger constructs via polypeptide-based crosslinkers present on the microunits' surface.¹²⁴ As an example of a specific tissue engineering strategy, the technique was applied for the fabrication of methacrylated chitosan and hydroxyapatite based osteon-like structures encapsulating osteoblast-like MG63 cells and HUVECs in a spatially controlled manner.¹²⁵ Photolithography can be further employed as a secondary technique for microcarrier production. For instance, electrospun fibres dispersed in a PEGDA precursor solution yielded cylindrical fibre-entrapped microgels upon localised photolithography and bare fibre dissolution. The main advantage here lies in the possibility to produce distinct compartment combinations within the same unit by sequentially stacking electrospun fibres with tailored compositions and/or bound growth factors.¹²⁶

Soft lithography

Soft lithography relies on printing and moulding mainly using elastomeric masters, which present the patterns of interest in bas-relief.¹²⁷ It encompasses several techniques such as microcontact printing, replica moulding, imprinting, microtransfer moulding, micromoulding in capillaries, and solvent-assisted moulding. For the production of microcarriers, replica moulding and imprinting are the most commonly applied soft lithography techniques. Both techniques can be used on a broader range of materials than photolithography. During replica moulding, the pre-polymer solution is cast onto the master and subsequently crosslinked. The resulting structure is dependent on the van der Waals interactions, wetting, and kinetic factors during mould filling.¹²² Replica moulding has been applied as a strategy to produce geometrically tuneable microconstructs encapsulating cells via photocrosslinking of a cell-laden pre-polymer solution.¹²⁸ A variation on replica moulding, particle replication in non-wetting templates (PRINT) produces isolated particles as the non-wetting surface confines the liquid precursor within the features of the mould. This technique may even be applied for a continuous, roll-to-roll production of high-resolution particles.^{129,130} Imprinting in turn relies on the thermoplastic properties of polymers and bypasses the need for photoinitiators. Due to the high temperatures generally required for the plastic deformation of a polymer, this technique is not compatible with cell encapsulation but presents itself as an attractive technique to produce microcarriers for cell anchorage.¹¹⁷ Replica moulding and imprinting are both simple and inexpensive methods to obtain microconstructs with a nanometric resolution, which can include topographical features.¹²² Nonetheless, the initial stamp generally relies on methods such as photolithography¹²⁷ or rapid prototyping techniques such as stereolithography¹³¹ to be produced. Interestingly, mould fabrication via an etching process originates Bosch etch lines as an artefact of the process. This may generally be considered a disadvantage of the process, yet it is in fact a relatively simple approach to tune geometry

and topography simultaneously. Upon PRINT, resulting cuboidal particles presented ridges on four faces, corresponding to the etch lines in the mould.^{132,133} A limitation of the imprinting and replica moulding technologies is the removal process of constructs. Options to circumvent this issue include sacrificial templates^{117,134} or responsive moulds with pneumatic-aid to enable recovery and minimise shape distortion.^{135,136}

Electron beam, ion beam, and multiphoton lithography

A further decrease in feature size and increase in nanoscale complexity requires the employment of alternative technologies. Electron beam and ion beam lithography are both maskless patterning techniques that allow to produce constructs with nanoscale precision. Electron beam lithography (EBL) provides a higher resolution and penetration depth than ion beam lithography (IBL), yet electron beam projections are susceptible to pattern distortion.¹³⁷ IBL presents the advantage of reduced scattering, resulting in higher patterning precision. These two techniques have in fact been combined where an initial EBL writing step was applied to produce nanopillars, which were subsequently sculpted via IBL. By leveraging the induction of structural changes in spider silk upon ion penetration, asymmetric complex microconstructs with nanoscale precision were produced while bypassing the need for potentially cytotoxic photoinitiators.¹³⁸

Another option is single-photon lithography, which applies a UV laser that photopolymerises a specific area in proximity with the focal point. A submicrometric x,y-resolution can be obtained, yet z-resolution is typically above 25 µm given the occurrence of initiation reactions above and below the focal plane. Using a near-infrared (NIR) laser source, multiphoton lithography relies on the two-photon absorption of NIR light to confine photoreactions to the focal plane, improving z-resolution to 2-3 µm. Multiphoton lithography enables a deeper sample penetration, yet is more time consuming and costly than single-photon lithography.^{139,140} The main limitation to produce cell encapsulating hydrogels via multiphoton lithography currently lies in the limited efficiency of available two-photon initiators, which should ideally be hydrophilic, water soluble, and present a molar absorptivity within the NIR range (800 nm).¹⁴¹

Electrodeposition

Electrodeposition is a versatile tool to produce cell encapsulating, geometrically diverse thin structures according to an exposure pattern that can be changed in real time by using a digital mirror device (DMD)-based system projecting CAD files. The system is composed of a photoconductive electrodeposition chip, a visible light supply coupled to a DMD, and a direct-current (DC) power supply.¹⁴² Alginate is a commonly applied biomaterial for the electrodeposition method given the non-cytotoxic and facile process of alginate crosslinking with divalent ions, such as calcium. Calcium-alginate electrodeposition is triggered at the electrode surface by the electrochemically induced release of calcium ions from calcium carbonate particles included in the initial alginate solution. Upon application of a direct current voltage to the

photoconductive chip, the DMD-based system limits light projection to a restricted area where ionic crosslinking of alginate occurs.¹⁴³ Crosslinked alginate structures, which may be laden with cells, can then be used as templates for liquefied-core capsule formation. Upon build-up of a multi-layered membrane via layer-by-layer technique with alginate, chitosan, and PLL, the alginate core is liquefied using calcium chelation. The final structure is a liquefied-core microcapsule that maintains the original form of the electrodeposited alginate.^{142–146}

Microfluidics

Microfluidics is the technique by which fluids are manipulated within channels with dimensions below the micrometric range. Via the manipulation of multiphase flows it enables the production of polymer particles, emulsions, and foams.¹⁴⁷ Commonly applied for the production of spheres, this technique may be employed to produce sphere deformation geometries such as rods, ellipsoids, and discs.¹¹⁸ Furthermore, by increasing the complexity of the system, more intricate shapes can be fabricated.¹²⁰ Coupling of the microfluidics system with photopolymerisation enables crosslinking of a photocurable resin or photosensitive polymer and subsequent collection of the produced particles. Continuous flow lithography supports the continuous generation micrometric hydrogels via photopolymerisation in a free-floating manner, where microgels are not adhered to a substrate, as opposed to what occurs in regular photolithography. Both the optical resolution and depth of field of the microscope objective condition the dimensions of obtained particles.¹¹⁸ However, this technique demands either short polymerisation times or slow flow rates, which requires highly concentrated prepolymer solutions and raises cytotoxicity issues. Stop-flow lithography appeared as an alternative to overcome this setback of continuous flow lithography while allowing cell-laden microgel production at a rapid rate. This technique relies on three steps, namely interruption of the liquid flow, followed by polymerisation of the patterned solution, and lastly particle flowing out of the device.¹¹⁹

Initially proposed systems for both continuous and stop-flow lithography within microfluidic channels relied on photomasks. Currently, microfluidics is combined with DMD-based technologies, termed optofluidics. High-speed optical projection systems are coupled with two-dimensional micromirror arrays, which control and projects UV exposure patterns according to linked computer aided design (CAD) files, circumventing the need for photomasks.¹⁴⁸ Furthermore, by inserting obstacles such as pillars and varying microchannel geometry, these systems are able to control inertial flow shaping, gravity-induced flow shaping, and UV light patterns to create truly complex geometries.^{120,149–152}

Table 1. Microcarrier geometries applied for drug delivery and tissue engineering strategies with corresponding material and production method.

Shape	Material	Production	Ref
-------	----------	------------	-----

Dimpled spheres	Polystyrene (PS)	Dispersion polymerisation	153
Spheroids, ellipsoids, and rods	Poly (lactide-co-glycolide) (PLGA)	Emulsion solvent evaporation	109–111, 154
Capped ellipsoids	Alginate with magnetic nanoparticles	Hanging drop crosslinking	155
Spheroids, cylinders, heart-shaped, rectangular, hexagonal, triangular prisms	Methacrylated chitosan, alginate, PCL	Superhydrophobic/superhydrophilic surfaces	112, 156, 157
Spheroids, ellipsoids, compartmentalised rods	Poly(methyl methacrylate) (PMMA), PS, polycaprolactone (PCL), ethoxylated trimethylolpropane triacrylate (ETPTA) and magnetic nanoparticles	Uniaxial stretching within sacrificial matrix	102–105, 108, 158
Hollow ellipsoids	Polydopamine, PS	Uniaxial stretching within sacrificial matrix. Posterior gas foaming or coating with polydopamine and PS leaking with tetrahydrofuran	106, 107
Barrel-, dumbbell-, and funnel-shaped	PEG, gelatin-methyl acrylate (GelMA), polyacrylamide (PAAm)	Material-dependent crosslinking while applying liquid bridge phenomenon between two surfaces	159
Cylinders	PLLA	Electrospinning and aminolysis	160
Rods and spheres with single or multiple protruding fibres	PLGA	Single and multiplexed electrospray	161
Cylinders, cubes, rectangular, hexagonal, and triangular prisms, arrow-, star-, Z-, cross-, donut-, plus sign-, and saw-shaped	Photocurable epoxy-resin SU-8, PEG, PEGDA, silk proteins (fibroin and sericin), alginate, gelatin, methacrylated hyperbranched polyglycerol, hydroxyapatite	Photolithography	115, 124, 125, 162–167
Cylinders, cubes, triangular prism, animal- (octopus, shark, butterfly), plus sign-shaped	ETPTA, PEG methacrylate, GelMA, and PAAm	Photolithography system with DMD	168, 169
Multi-compartmentalised cylinders	PEGDA hydrogel containing PLGA fibres	Electrospinning and photolithography	126

LEGO bricks and complex geometries	Genetically engineered spider silk	Combination of IBL and EBL	138
Helicoids	Methacrylamide chitosan or GelMA containing iron oxide nanoparticles	Multiphoton lithography	170, 171
Helicoids	Alginate/PEGDA containing magnetic nanoparticles	Microfluidic spinning and coiling technology	172
Cylinders, hexagonal, triangular and rectangular prisms, keyboard character-shaped, complex shapes (characters, puzzles, barcodes, smiling faces, ring-over-disc, cross, yin-yang, three-discs-over-a-bar, circle-over-wrench, assembled triangular, assembled zigzag, and assembled quadrilateral)	Collagen type I, sPEG-A with SPIONs, methacrylated hyperbranched polyglycerol, hyaluronic acid, PEGDA, PLGA, commercial photosensitive resin	Replica moulding	67,1 16,1 28,1 67,1 73– 176
Cylinders and rectangular prisms	Agarose	Replica moulding with thermoresponsive PNIPAAm moulds	177
Cylinders	PLGA	Solvent/non-solvent plasticization replica moulding	178
Cylinders, pentagonal, triangular and quadrangular prisms, plus- and hepatic lobule-shaped. Cylinders with cylindric, rectangular, and triangular cut-outs	Collagen type I, gelatin, agarose, and matrigel	Pneumatic-aided replica moulding	135, 136
Cubes, cylinders, grooved cubes	PEG; combination of ETPTA, cystaminebisacrylamide, aminoethyl methacrylate, doxorubicin, and hydroxycyclohexylphenyl ketone; combination of albumin and insulin	PRINT	132, 133, 179
Nanogrooved microdiscs (“topodiscs”), cubes, donut-, and LEGO-shaped	PCL, poly(d,l-lactic acid) (PDLLA)	Imprinting	117, 134
“Spiky” microparticles	Alginate, polyethylene glycol (PEG) and dextran	Aqueous two-phase based microfluidics	180

Ellipsoids, truncated spheres, hemispheres, tear-, and bullet-shaped, rods, cylinders, rectangular, hexagonal, and triangular prisms, rings, keyhole-shaped	Alginate, PEGDA, PEGDA with magnetic nanoparticles, PLGA, tripropyleneglycol diacrylate, ethyleneglycol dimethacrylate, 1,6-hexanediol diacrylate, dimethacrylate oxypropyl dimethylsiloxane, divinylbenzene, ethyleneglycol diacrylate, pentaerythritol triacrylate	Continuous flow lithography microfluidics	113, 114, 188, 189, 118, 181– 187
Cylinders, cubes, rectangular, pentagonal, hexagonal, and triangular prisms, donut-, cross-, and S-shaped	PEGDA, 3-(trimethoxysilyl)propyl acrylate:ethoxy trimethylolpropan	Stop-flow lithography microfluidics	119, 190– 192
Bell-, bullet-shaped	PEGDA with magnetic nanoparticles	Non-uniform UV stop-flow lithography microfluidics	193
Wrinkled-surface cylinders, heart- and deformed rhombus-shaped	PEGDA	Stop flow lithography with wrinkling post-process	194
Complex shapes, cubes, triangular and rectangular prisms, star- and L-shaped	PEGDA, GelMA	Optofluidic fabrication in regular or non-rectangular microfluidic channels	120, 149– 152
Hollow hexagonal-, gear-, donut, square frame-, dumbbell-, rod-, and hepatic lobule-shaped	Alginate, chitosan, and PLL	Photo-induced electrodeposition and layer-by-layer	142– 146

3D application of geometrical and topographical cues

Tissue engineering

Top-down versus bottom-up.

Tissue engineering strategies for 3D cell culture can roughly be divided into two approaches: top-down and bottom-up. In top-down strategies, a prefabricated scaffold is populated with cells, which are expected to migrate within the scaffold and create their own extracellular matrix (Figure 5). Scaffolds are often coupled with systems for aided perfusion, bioactive molecules such as growth factors, and even mechanical stimulation.¹⁹⁵ However, the restrictive architecture and geometry of top-down scaffolds are an impediment for optimal

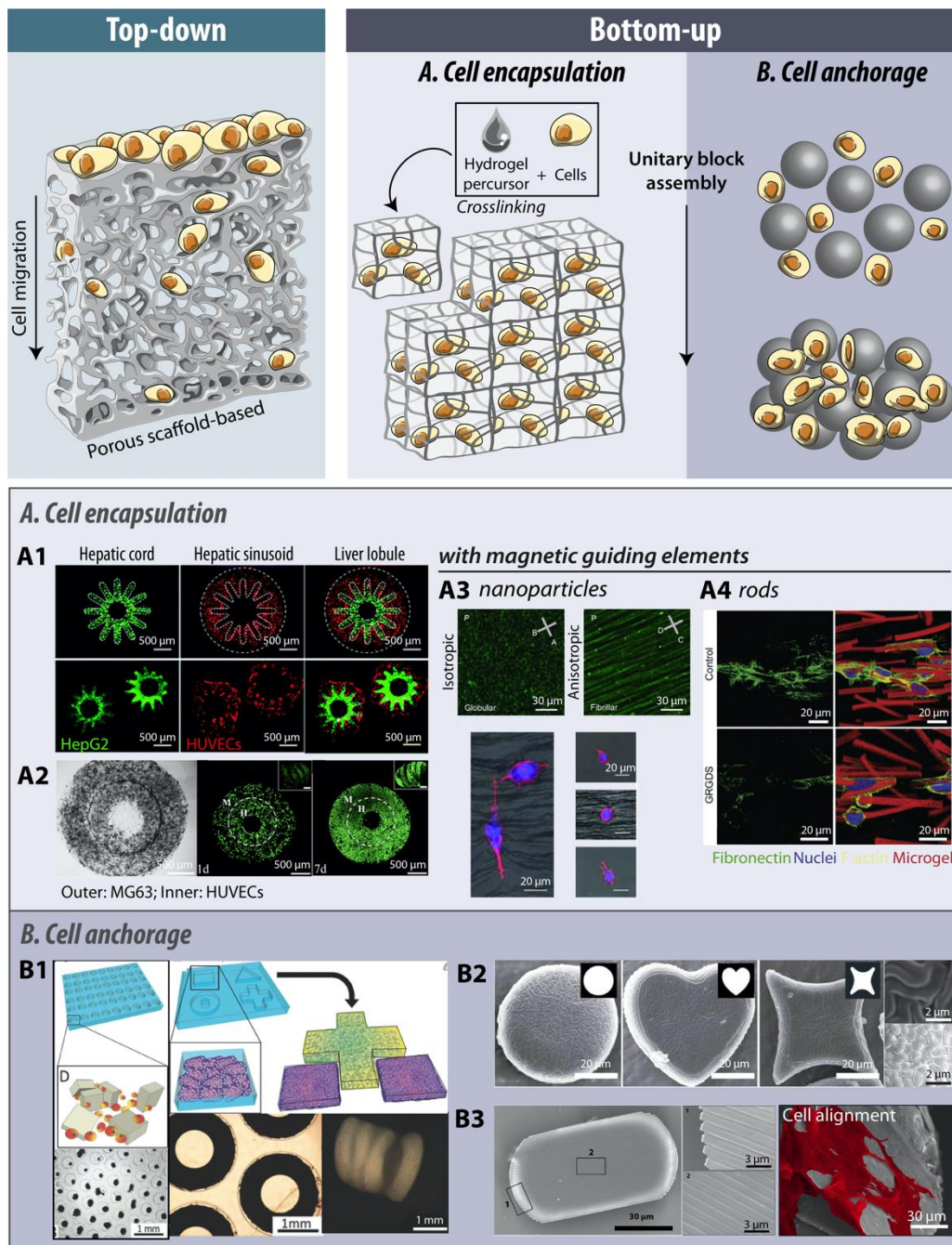


Figure 5. Schematic representation of top-down versus bottom-up tissue engineering strategies. Bottom-up cell encapsulation (A) and cell anchorage (B) approaches. [A1. Reprinted with permission from ¹³⁵, Copyright (2016) Royal Society of Chemistry. A2. Reprinted with permission from ¹²⁵, Copyright (2015) American Chemical Society. A3. Reprinted with permission from ¹⁷³, Copyright (2018) Elsevier. A4. Reprinted with permission from ²²⁴, Copyright (105) John Wiley & Sons. B1. Reprinted with permission from ¹¹⁵, Copyright (2014) John Wiley & Sons. B2. Reprinted with permission from ¹⁹⁴, Copyright (2016) Springer Nature. B3. Reprinted with permission from ¹¹⁷, Copyright (2019) Royal Society of Chemistry.]

cell culture, limiting mass transfer and hindering the production of a functional histoarchitecture.¹⁹⁶ Cell migration is also restricted within these systems, resulting in an inhomogeneous cell distribution throughout the scaffold.¹³⁴ Furthermore, when considering engineering vascular tissues, vascularisation of top-down fabricated constructs has proven to be challenging.¹⁹⁶ In fact, one of the major difficulties in TE is to develop a vascular network, capable of sustaining the requirements of the engineered tissue. Whereas perfusion bioreactors can be used *in vitro* to enable an adequate diffusion within large constructs,

upon implantation, a functional vasculature is required to supply oxygen and nutrients to the entire engineered construct. Since vascular ingrowth of host blood vessels to the construct is a slow process, cells within large-scale, non-vascularised constructs will likely suffer from nutrient deficiencies and/or hypoxia.¹⁹⁷

Bottom-up appears as an alternative to the traditional top-down approaches, where smaller, often micrometric carriers, are assembled, either in a random or controlled manner, to form larger structures (Figure 5).¹⁹⁵ With these microcarriers,

cells can either be encapsulated within the core (Figure 5A), or adhere to the exterior of the microcarriers (Figure 5B). Bottom-up strategies enable a homogeneous cell seeding and have the added advantage of allowing to spatially control the distribution of cell-laden modules with the aim of acquiring a functional histoarchitecture.^{196,198} Recent trends point towards the use of minimalist “low material” approaches, which enable cell self-organisation while delivering biochemical and biophysical cues for an optimal tissue regeneration.¹⁹⁹ Polymeric spherical systems for both cell encapsulation and cell anchorage have been extensively studied and reviewed previously.^{200,201} Materials used in such systems range from naturally derived materials, such as chitosan²⁰² and alginate,²⁰³ to synthetic materials, such as polycaprolactone²⁰⁴ and poly(ethylene) glycol–vinyl sulphone.²⁰⁵

Cell encapsulation within micron-sized hydrogels for minimal invasive implantation is an example of a bottom-up approach. Micron-sized hydrogels were first reported in 1980 for the immunoisolation of pancreatic islets.²⁰⁶ Since then, developing and exploring microencapsulation techniques has received increasing interest. Due to their tuneable mechanical properties and degradability, hydrogels present themselves as optimal vehicles for cell encapsulation. Encapsulated cells are protected from the exterior environment and, via engraftment of polymer chains with peptide motifs, when necessary, cell attachment and long-term proliferation is enabled.²⁰⁷ Typically applied for encapsulation of multiple cells simultaneously, these systems may also be used to envelope single cells.²⁰⁸ However, for constructs typically above a maximum diffusion distance of 200 μm , diffusion of oxygen and nutrients to cells within the hydrogel core is impaired, leading to the formation of a necrotic core.^{209,210} To overcome this drawback, strategies to include pores within hydrogels, such as porogen leaching, electrospinning, among others, have been explored.¹⁹⁹ Another option is to use chemical bonding via PEG-NHS annealing of previously produced cell-laden microgels, resulting in an inherently porous structure due to the interstitial spaces formed between spherical microgels.²¹¹ Such structures are commonly referred to as bead-based or granular scaffolds and have been recently reviewed elsewhere.²¹² Liquefied-core capsules are likewise an attractive option where cells are cultured in a compartmentalised liquid environment, with facilitated diffusion comparatively to jellified environments.²¹⁰ The embedding of microfluidic networks within the hydrogel network via bioprinting, soft lithography, or fibre templating may also improve diffusion.²¹³

Whereas polymeric microparticles of spherical or other geometries may be applied for cell encapsulation, an alternative is to use these platforms as anchoring points.^{19,214,215} The surface of microcarriers may be tuned both biochemically and physically.²¹⁶ Selective cell anchoring capabilities have been imparted onto spherical microcarriers via the immobilisation of specific monoclonal antibodies for either endothelial or stem/stromal cells, allowing to separate and capture the desired cell population.²⁰² Via physical modification, anchorage microcarriers can be imparted with topographical and geometrical cues to control cell fate. To this end, nanogrooved

microdiscs, “topodiscs”, directed cell fate towards the osteogenic lineage simply due to the topographical cues present on the surface of these tailored disc-shaped particles.¹¹⁷ Whereas the assembly of anchorage-dependent bottom-up approaches may be cell-mediated,²⁰² they may also rely on chemical crosslinking. Both enzyme- and ultraviolet light-mediated annealing of spherical microgels have been previously applied to develop injectable bead-based scaffolds with tuneable geometry, which could anchor cells. The size of applied microgels governs pore size and consequently controls cell migration throughout the scaffold.^{205,217}

A combination of cell encapsulation and anchorage was established where cell-laden microgels were subsequently coated with a distinct cell population. This strategy aimed to produce a pre-vascularised network that could anastomose upon implantation.²¹⁸ Ultimately, bottom-up strategies can be used to interweave a pre-vascularised network between cell-seeded micrometric structures in a precise manner, something which would not be possible with top-down strategies.²¹⁹

Due to the micrometric nature of units applied for bottom-up strategies and their proximity in size to cell dimensions, this unlocks several opportunities to tailor and guide cell response via biophysical signals such as geometrical, mechanical, and topographical cues. An interesting approach relied on the use of microcontact printing to spatially position polyelectrolyte multilayers or PLGA microfilms. The geometry for these thin films ranged from 2 μm microparticles to millimetre long fibres. Upon cell adhesion to micropatterned sections, the temperature-sensitive sacrificial layer allowed to collect cell-loaded constructs, which then assembled as cell-microparticle aggregates or mesh-supported cell sheets.²²⁰ Considering the fibrous environment of the ECM, microfibres appear as attractive biomimetic tissue engineering substrates. The techniques used to produce these fibres and their applications have been previously reviewed.²²¹ Additionally, fibres can be tailored via the introduction of topographical features, such as grooves, which opens up a multitude of possibilities.²²²

Cell encapsulation.

Living tissues are generally composed of different cell types, which are organised in tissue specific conformations. In order to mimic these geometrical patterns, tissue engineering approaches must resort to strategies that allow to spatially control cell organisation.¹⁶⁵ As has been previously stated, several techniques can be used to produce cell-laden constructs with relevant geometries.

Cell-encapsulating hydrogels with varying geometry have to some extent been explored as proof of concept and produced using distinct techniques. For example, oxidised methacrylated alginate cylindric microgels produced via microfluidics have been shown to be a viable option for chondrocyte encapsulation.¹¹³ Pneumatic-aided replica moulding has been applied to produce cell-laden microgels with well-defined geometries, bypassing replica moulding issues related with deforming constructs upon production.^{135,136} DMD coupled photolithography enables the cell encapsulation within butterfly- and cross-shaped microgels (approx. 300 μm

width).¹⁶⁸ Cylindric and rectangular prism shaped liquefied capsules produced via a combination of electrodeposition, layer-by-layer, and core liquefaction are too promising candidates for cell culture.¹⁴⁵ Another approach relies on the use of superhydrophobic surfaces with hydrophilic regions with different shapes. This method granted the encapsulation of cells within thin alginate microgels of various shapes (cylinders, heart-shaped, rectangular, hexagonal, and triangular prisms) with diameter/length of 3 mm. Comparatively to bulk hydrogels with 2 mm thickness, thin alginate films produced via this method presented a significantly increased cell viability and metabolic activity.¹⁵⁶ Furthermore, the inclusion of magnetic nanoparticles enabled cell-laden microgel manipulated by an external magnetic field.^{155,156,223}

Even though mentioned studies produce microgels with specific geometries, few or no comparisons have been made between geometries on aspects such as cell viability or proliferation. To this end, the effect of varying circularity of methacrylated chitosan hydrogels from spheres to spheroids on the viability of encapsulated L929 cells was studied. Specifically, oblate ellipsoidal hydrogels with smaller short axis presented a higher cell viability than spheroids with longer short axis or spheres. Since spheroids possessed a higher surface area to volume ratio, this likely facilitated oxygen and nutrient diffusion to encapsulated cells.¹¹²

Co-culture cell encapsulation strategies have similarly been explored. Replica moulding with PDMS moulds was employed to produce adhered or free-standing collagen hexagonal prisms with encapsulated fibroblasts. By seeding a second collagen precursor to fill the gaps between crosslinked hexagons, the authors produced coplanar arrays of fibroblasts pre-labelled with distinct fluorescent dyes, demonstrating its potential for the inclusion of distinct populations of cells. Moreover, several layers could be stacked to form a larger construct.¹¹⁶ In turn, thermoresponsive poly(N-isopropylacrylamide) dynamic micromoulds were applied to fabricate compartmentalised cell-laden microgels shaped as cylinders or rectangular prisms. The strategy involved crosslinking fibroblast- or HepG2-laden agarose microgels within the mould and subsequently leveraging its thermoresponsive behaviour to induce expansion, allowing for the deposition and crosslinking of an outer HUVEC-laden layer.¹⁷⁷ Similarly, pneumatic-aided replica moulding was applied to produce cylindrical collagen microgels containing single or multiple channels with distinct geometries (squares, triangles, or circles) to ensure a higher oxygen and nutrient diffusion. Multi-compartmental microgels were similarly produced, containing at the core cylindric, rectangular, or triangular prism shaped hydrogels encapsulating HepG2 cells, fibroblasts, or A549 cells, and enveloped by a semi-spherical HUVEC laden microgel.¹³⁵ Alternatively, HUVEC coating of collagen type I cylinders encapsulating HepG2 cells, assembled within a larger construct and perfused with cell culture medium or whole blood, demonstrated that HUVEC presence led to an increased clotting time and reduced thrombogenicity.¹⁷⁴

Aside from microunit fabrication, another key aspect of the bottom-up strategy lies in the assembly process. To this end,

“lock and key” assembly is an option to group compatible shapes that have been previously produced via methods such as photolithography,^{164,165} electrodeposition combined with layer by layer and core liquefaction,¹⁴³ crosslinking within two surfaces (liquid bridge phenomenon),¹⁵⁹ or microfluidics.¹⁵¹ By placing microgels under agitation, compatible shapes aggregate via a “lock and key” type assembly.¹⁶⁵ Similarly, acoustic waves induce microgel self-assembly, where parameters such as acoustic frequency and amplitude can be optimised.¹⁶⁴ Optically induced dielectrophoretic manipulation likewise allows to assemble microgels with distinct geometries (cubes, triangular and rectangular prisms, L- and star-shaped), laden with distinct cell populations, in a “tetris”-like manner.¹⁵¹ Self-locking donut- and dumbbell-shaped liquefied microcapsules containing cells within the core have also been reported. For that, alginate constructs with the corresponding shape were produced via electrodeposition combined with layer by layer and core liquefaction. Whereas the layer-by-layer process caused shrinkage, which allowed to fit the dumbbell within the donut, liquefaction-induced microcapsule swelling allowed to achieve self-locking of both shapes.¹⁴³ Alternatively, chemical assembly can be applied to group cell-laden microgels with different geometries (cubes, cylinders, and star-shaped). This was performed via a Michael-type addition reaction between the acrylate groups on microgel surfaces and the thiol groups on the crosslinker. Interestingly, constructs fabricated by the assembly of star-shaped microgels presented higher porosity, permeability, and interconnectivity when compared with constructs produced with cubic and cylindric microgels. This technique could hence be useful to produce larger constructs with tuneable properties.¹²⁴

Moreover, strategies to guide the spatial distribution of cells within hydrogel structures have been recently explored. These strategies generally include magnetic nanoparticles and rely on a magnetic field to control their distribution and orientation, upon which the hydrogel network is crosslinked in place. Moreover, the mechanotransduction pathways set in motion by these hydrogel-embedded cues have been subjected to a greater analysis than solely the role of geometry. Aligned topographical features were produced within a 3D hydrogel matrix via magnetic field directed self-assembly of magnetic nanoparticles into chains. Nanoparticles were coated with distinct proteins (fibronectin, laminin, or BSA) to mimic ECM fibres and parameters such as chain length, width, and interchain distance were controlled. In this case, fibroblasts encapsulated within aligned nanoparticle loaded Matrigel tended to have more extended dendrites directed parallelly or perpendicularly to chains as opposed to conditions with randomly distributed nanoparticles.²²⁴ Using the same model, it was determined that the generation and length of fibroblast's protrusion was dependent on the expression of integrin β_1 and fascin, yet co-alignment with engineered fibrils was still verified independently of their knock-out. Conversely, protrusion length upon myosin II inhibition with blebbistatin remained unchanged, while protrusion orientation was markedly random (Figure 5A3).²²⁵ Given the role of myosin II in the deformation of cell shape by generating contractile tension via actin filament

pulling, this study links cell contractility with the sensing of topographical cues in a 3D environment.^{225,226} Following a similar strategy, another study incorporated rod-shaped magnetic inert or peptide-coupled microgels within bioactive fibrin or inert PEG hydrogels (Figure 5A4). Whereas fibroblasts in fibrin hydrogels aligned independently of microgel surface chemistry, a striking increase in fibronectin production was observed for bioinert microgels. Fibronectin co-localisation with vinculin led to conclude that with inert microgels, cells were required to produce their own ECM for attachment. Nuclear YAP localisation increased with higher microgel content and with peptide-coupled microgels, pointing to a stronger interaction of cells with peptide-coupled microgels. Within PEG hydrogels, biofunctionalized microgels were required for cell attachment and spreading, whereas almost no fibronectin was produced with inert microgels.¹⁷³

Strategies for bone and liver tissue engineering have been particularly explored in the literature. Such approaches, which generally take advantage of geometry to replicate osteon- or lobule-like structures and feature compartmentalised distribution of distinct cell populations, are described in the following subsections in more detail.

Liver. Aiming to replicate the architecture of a biomimetic lobule-like microtissue, a system consisting of the compartmentalised encapsulation of HepG2 cells and HUVECs was developed. To this end, HepG2 cells were seeded within the core in a hepatic cord-like geometry whereas HUVECs were seeded in a hepatic sinusoid-like geometry (Figure 5A1). Upon treatment with analgesic drug acetaminophen, which is known to induce hepatotoxicity, the lobule-like microtissue formed was shown to be more sensitive to acetaminophen when compared with a HepG2 monoculture in both 2D (monolayer) and 3D (encapsulation in collagen hydrogel) conditions. Hence, the developed microtissue could in fact be a useful 3D tissue model for *in vitro* drug toxicity screening.¹³⁵ However, the results obtained could be mostly attributed to the co-culture and not geometry of the constructs *per se*.

Another approach to produce hepatic lobule modules relied on a gear-shaped geometry, where alginate constructs containing RLC-18 rat liver cells were initially produced via electrodeposition. Upon detachment, modules were coated with PLL to form an outer shell and the alginate core was liquefied to originating microcapsules. When comparing gear-shaped modules (975 μm diameter with a 300 μm height) and cylindric modules (840 μm diameter and 400 μm height), an increased albumin and urea secretion was observed for gear-shaped modules at more advanced timepoints, demonstrating a higher hepatic function. This study in fact highlighted the role of geometry on hepatic function but failed to determine the mechanotransduction pathways activated in the process. In addition, gear-shaped modules could be further assembled into 3D four-layered hepatic lobule models.^{144,146} Aiming to take this concept a step further into a co-culture system, the outer shell of fibronectin coated gear-shaped microcapsules containing HepG2 cells was posteriorly seeded with fibroblasts. Fibroblast adhesion to the exterior of constructs enabled a continuous

increase in urea and albumin secretion and, upon lobule module stacking, mediated construct self-bonding.¹⁴²

Bone. An approach to produce an osteon-like structure relied on the compartmentalised encapsulation of human osteoblast-like cells (MG63) and HUVECs within alginate and gelatine hydrogels. MG63 or HUVEC laden microgels were fabricated using photolithography and assembled via a “lock and key” assembly for cylindric and cross-shaped microgels, or a “concentric double-ring” assembly for donut-shaped microgels.²²⁷ Taking this concept further, osteon-mimetic concentric double-ring structures (2 mm outer diameter) were produced using methacrylated chitosan and hydroxyapatite. The inner ring contained HUVECs whereas the outer ring contained MG63 cells (Figure 5A2). The osteogenic and angiogenic potential of the co-culture system was evidenced by a significantly increased collagen I and VEGF expression, as well as a slight increase in ALP and osteocalcin expression when compared to the monoculture system.¹²⁵ The benefits of a co-culture system composed of osteoblasts or stromal cells in combination with endothelial cells for the formation of bone-like tissue have been previously proven.^{228,229} Hence, an interesting approach would be to compare the expression of specific bone and vascularisation markers for distinct geometries. By controlling cell localisation within hydrogels and playing with different geometries, it would be possible to take a step forward in pinpointing the role of geometry and its specific impact on the outcomes observed. Given the impact of actomyosin contractility in osteogenic differentiation, the effects of tension in a 3D context were studied. Using a combination of osteogenic and adipogenic factors, MSCs encapsulated within hydrogels preferentially differentiated into the osteogenic lineage at the edge of hydrogels, whereas cells localised in central regions underwent adipogenesis. Upon treatment with blebbistatin, a myosin II inhibitor, a considerable decrease in osteogenesis was observed, which allowed to link this occurrence to an increased actomyosin contractility in the hydrogel periphery. Moreover, by expressing ROCK3 so as to increase myosin activity, a thicker layer of cells differentiated into the osteogenic lineage was observed.⁶⁷

Cell anchorage.

As previously stated, microcarriers as anchoring points for cells are another attractive option bottom-up approach. RGD-coupled PEGDA microrods (length 150-450 μm) were shown to enable fibroblast adhesion and led to the formation of larger aggregates via a cell-mediated bottom-up assembly.¹⁸⁸ Via reeling of magnetic alginate fibres, ring structures (diameters of 40 or 160 μm) were produced and seeded with fibroblasts, which aligned along the longitudinal direction of fibres and acquired a spindle-shaped morphology. Cell-seeded microrings could additionally be stacked via non-contact magnetic micromanipulation to form larger constructs (Figure 5B1).²³⁰ In line with this, helicoidal cell-seeded microcarriers may be assembled via translational corkscrew motion, activated by a rotating magnetic field, to form double or triple helix structures, while staining cell survival.¹⁷²

Cubes ($40 \times 40 \times 40 \mu\text{m}^3$), rectangular prisms ($80 \times 80 \times 40 \mu\text{m}^3$) and plus sign-shaped ($90 \times 90 \times 40 \mu\text{m}^3$) micro-objects produced using a photocurable resin have been demonstrated to enable a cell-mediated assembly of micro-objects into larger constructs. Upon placement of constructs into toroidal-shaped moulds, cells could further mediated construct fusion into millimetre-sized toroids, which could in turn be stacked to form tubular structures.¹¹⁵ “Low material” strategies such as ultrathin PCL microparticles with varying geometry have also been shown to enable a cell-mediated assembly and even particle folding to generate 3D constructs.¹⁵⁷ When comparing donut-shaped and cubic geometries for culturing of hMSCs, a similar cell viability with both types of micro-objects was observed. Theoretically, donut-shaped objects should introduce more pore volume into the resulting aggregate and consequently impact oxygen and nutrient diffusion, yet this appeared not to be the case. Upon mono or co-culture of hMSCs and HUVECs with cube-shaped objects, the authors concluded that cell type and order of cell seeding with cubes determined aspects such as compaction rate, cellular organisation, and cell survival. For instance, hMSC-only aggregates with cubes presented a higher compaction for increased object-to-cell ratios (e.g., more compact aggregates for a 1:20 than for a 1:8 ratio), whereas HUVEC-only conditions resulted in minimal aggregate formation for both ratios studied. For co-culture conditions, sequential seeding of HUVECs with pre-aggregated cubes and hMSCs led to more robust constructs with an increased HUVEC adhesion when compared with a simultaneous seeding of HUVECs, hMSCs, and cubes.¹³⁴

An advantage of anchorage versus encapsulation systems is the fact that topographical cues can easily be introduced onto the surface of microcarriers. Whereas encapsulations systems are so far limited to the magnetic manipulation of rods or fibre-like structures to control cell alignment from within,^{173,224,225} anchorage microcarrier systems can be modified prior to cell contact. Given the well-established impact in a 2D context of topographical features on cell orientation, migration, cytoskeletal organisation, differentiation, as well as inter- and intracellular signalling, transposing these cues to the third dimension is of the utmost importance, since it better mimics the native cell environment.^{231,232} The role of nano and microscale topographical features in a 2D environment have been previously reviewed.^{28,233,234} Yet to date, few strategies have incorporated topographical features onto microcarriers. Wrinkled topography has been introduced onto non-spherical particles by partial curing of the superficial polymer layer, which was subsequently wrinkled via plasma treatment (Figure 5B2). An increased cell adhesion was observed for wrinkled surface particles and, considering that both smooth control and wrinkled particles were submitted to plasma treatment with no significantly different surface chemistry, this enhanced adhesion was attributed to the topographical cues.¹⁹⁴ Additionally, nanogrooved microdiscs, “topodiscs”, have been proposed. These micron-sized platforms for a bottom-up cell-mediated assembly were produced via imprinting and possessed a disc-like shape featuring surface nanogrooves (Figure 5B3). Due to the enhanced surface area to volume ratio when compared with conventional spherical microparticles,

topodiscs led to an increased cell proliferation. More importantly, these tailored microdiscs stimulated the osteogenic differentiation of hASCs without requiring supplemental osteoinductive factors added in the culture medium.¹¹⁷

Drug delivery and cell targeting

Spherical microparticles are among the most studied and widely applied geometries for controlled delivery of pharmaceuticals and bioactive agents. This is likely due to the ease of fabrication, whether by microfluidics,²³⁵ oil-in-water emulsion,²³⁶ solvent emulsion evaporation,²³⁷ superhydrophobic surfaces,²³⁸ electrospray,²³⁹ among others. Drug-encapsulating microparticles may roughly be divided into two categories: reservoir/core-shell systems, and matrix/monolithic systems. Controlled release from microparticles is impacted by factors such as drug diffusion out of the device, polymer swelling or erosion, osmotic effects, etc. Initial drug concentration is also a preponderant factor, with differing release profiles for microparticles encapsulating drugs below or above their solubility.²⁴⁰

However, spherical microparticles may not always be the most advantageous geometry. For instance, distinct particle morphologies present altered polymer matrix degradation rates, consequently allowing to tailor drug release kinetics¹⁶¹. As such, for the same volume of a spherical microparticle, distinct geometrical shapes such as cubes or spheroids will present an increased surface area, which may facilitate diffusion across the particle surface. Taking only diffusion into consideration, numerical modelling studies assessed the impact of geometry for the same particle volume on the release profile of a specific compound. For modelled geometries (spheres and spheroids), it was determined that spheroids with smaller short axis presented a faster release and reached a plateau more rapidly than spheroids with larger short axis and even faster than spheres. This trend was experimentally corroborated, as the release kinetics of model protein BSA from chitosan spheroidal hydrogels was faster than from spherical hydrogels with the same volume.¹¹² The loading capability of PLGA spheroids and ellipsoids with paclitaxel,^{109,110} BSA,¹¹⁰ and model peptide drug octreotide acetate¹¹¹ has been established, still the impact of varying shape on the release profile has yet to be explored. Applying a sequential process, bi-compartmental fibre-entrapped cylindric hydrogels (approx. $200 \mu\text{m}$ diameter) were produced. Firstly, PLGA fibres loaded with either bFGF or BMP-2 were produced via electrospinning and sequentially stacked. Secondly, PEGDA-entrapped fibres were produced via photolithography, which yielding individual cylindric microgels upon the dissolution of bare fibres. By using a distinct lactide/glycolide ratio for bFGF- or BMP-2-loaded fibres, a tailored release of either compound could be achieved.¹²⁶

The selection of the production method is key so as not to interfere or diminish the activity of the encapsulated drug/bioactive agent. Since liquid phase organic solvents may impact drug activity, an option is to use solvent plasticisation with a vapour mixture. This method was applied to produce

cylinders by the deformation of initially spherical VEGF-loaded PLGA microparticles within 200 μm diameter cylindric moulds, while successfully maintaining VEGF activity. When cultured with HUVECs it was anticipated that due to their higher surface area and thus expected faster VEGF release, cylinders would increase the sprout number comparatively to microspheres. This however did not occur and was attributed to the low aspect ratio of cylinders and to a possible degradation at longer culturing timepoints.¹⁷⁸

Tumour tissues present highly reducing intracellular environments and high GSH (γ -glutamyl-cysteinyl-glycine tripeptide) levels, which can be harnessed for targeted delivery. Whereas disulfide bonds are stable in the presence of low GSH levels, a rapid cleaving via GSH-mediated thiol-disulfide exchange reaction occurs with high GSH levels.²⁴¹ Taking advantage of this fact, doxorubicin-loaded cuboidal particles (side length 2 μm) crosslinked with disulfide were applied to selectively target HeLa cervical cancer cells.¹³³ Alternative tumour targeting strategies have applied helicoidal magnetic microparticles, or “microswimmers”, which showed promising results due to their steerability under a rotating magnetic field. These 20 μm long helicoidal structures composed of methacrylamide chitosan and magnetic nanoparticles were produced via two-photon polymerisation and could be loaded with doxorubicin, which was released locally on-demand under an external light stimulus (Figure 6A).¹⁷⁰ This system has also been used for targeted cell labelling for therapeutic intervention of ErbB 2 overexpressing SKBR3 cancer cells. Taking advantage of the local elevated MMP-2 concentration in cancer sites and the degradability of gelatine to this enzyme, local delivery of anti-ErbB 2 antibody-tagged magnetic contrast agents may be induced by using magnetic gelatine methacryloyl microswimmers.¹⁷¹ Synthetic nano/micro-motors, capable of movement via bubble and acoustic propulsion or light-driven motion, are gaining significant interest in the biomedical field due to their response to external stimuli.^{242,243}

A practical application for microcarriers with distinct geometries is their potential for shape-mediated, or “lock and key” assembly. Shapes such as cylinders, cubes, and triangular prisms are easily manufactured by a combination of photolithography with a dynamic photomask to generate compatible “parent” and “daughter” particles laden with different viruses. Initially, “parent” particles were assembled within PDMS moulds according to their shape. Subsequently, smaller “daughter” particles fit within the shape-dependent indentations of “parent” particles (e.g., triangular prism fits within larger rectangular prism with triangular cut-out). Cells seeded atop of the “daughter”/“parent” microscale self-assembling were spatially subjected to gene transfection. Due to the loading of “parent” and “daughter” particles with distinct viruses, it was possible to locally produce heterogeneous cell populations in a controlled manner (Figure 6B).¹⁶⁹

Taken together, considering geometry in the design of strategies for drug delivery and cell targeting presents several advantages. Yet it is crucial to assess the scalability and inherent costs of such strategies for a successful entry into the clinical setting.

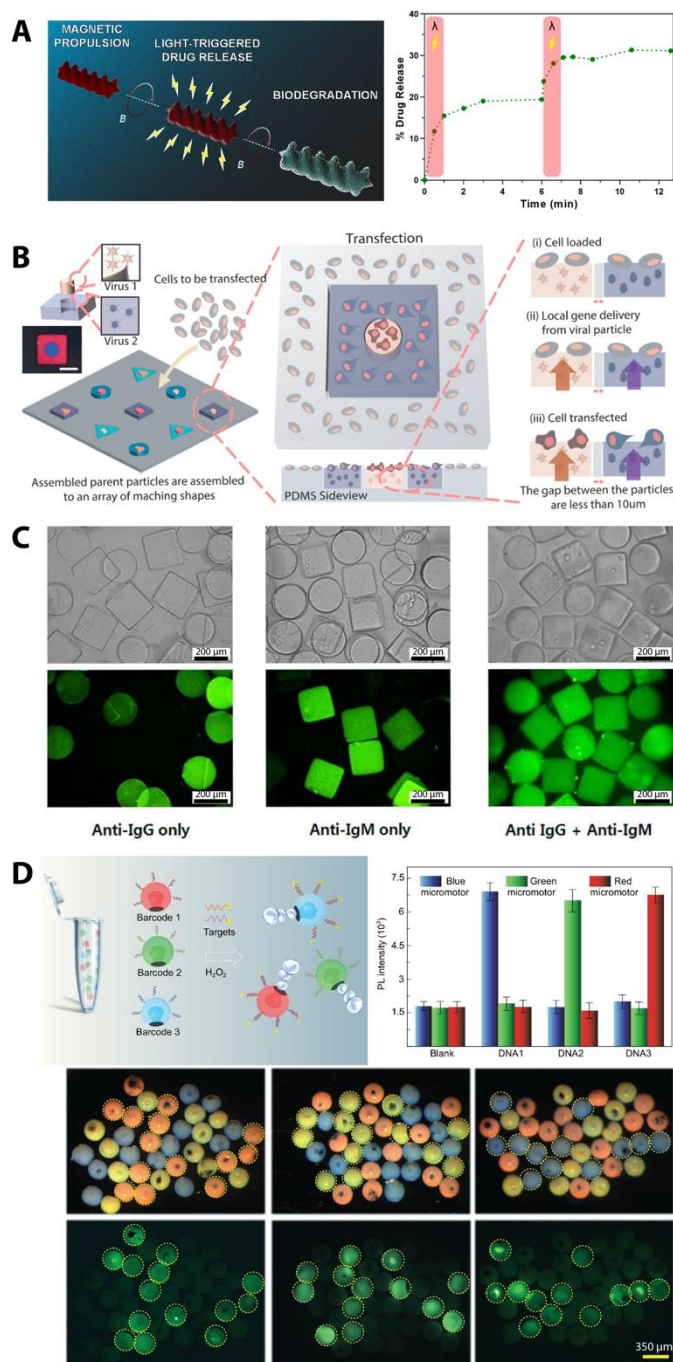


Figure 6. A. Magnetically powered, double-helical microswimmers with light-induced drug [Reprinted with permission from ¹⁷⁰, Copyright (2018) American Chemical Society]. B. Geometry-dependent assembly of “daughter/parent” particles for localised cell transfection [Reprinted with permission from ¹⁶⁹, Copyright (2018) AIP Publishing]. C. Multiplexed immunoassays using shape-coded hydrogel microparticles immobilizing distinct proteins [Reprinted with permission from ¹⁶², Copyright (2012) MDPI]. D. Multiplex detection of three target DNA via fluorescence using structural color-barcode micromotors [Reprinted with permission from ²⁴⁷, Copyright (2020) Oxford University Press].

Biosensors

One-step microfluidic biosensors have been based on the application of cylindric microgels. Microgels containing glucose oxidase and peroxidase were fabricated within the polymerisation chamber of a microfluidic chip and then sent via

a pressure-driven flow to the connected reaction chamber. Upon feeding a glucose and Amplex Red solution to the microfluidic system, glucose oxidase mediated the conversion of glucose into gluconolactone and hydrogen peroxide, whilst the latter in conjunction with peroxidase reacted with Amplex Red to produce fluorescent resorufin. With this system, it was possible to correlate fluorescent intensity with glucose concentration over a physiologically relevant range. Additionally, for the same glucose concentration, smaller or larger microgels resulted in a rapid lower fluorescence intensity or slower high fluorescence intensity, respectively.¹⁶⁶

Geometry has also been useful for multiplex assays, namely miRNA profiling using geometric barcoding. This strategy relied on the combination of high-resolution imaging with programmable DNA origami nanostructures presenting pre-designed nano-array patterns for multiplexed capture.²⁴⁴ Similarly, surfaces with programmable wettability may be applied for 2D encryption of fluorescence information due to selective capture and release of hydrogel particles.²⁴⁵ Furthermore, in response to the growing demand for high-throughput and high-content protein analysis, protein microarrays have been developed to identify different proteins simultaneously. Commonly used systems are composed of optically coded spherical microparticles, yet these are limited to the number of colour combinations and possible spectral overlaps. Hence, shape-coded suspension protein microarrays appear as an alternative to the traditional colour-coded options. Cylindric microgels were immobilised with IgG whereas rectangular prism microgels were immobilised with IgM. When reacted with samples containing varying mixtures of FITC-anti-IgG and FITC-anti-IgM, a simultaneous detection of IgG and IgM without crosstalk induced by the fluorescence indicator was possible (Figure 6C).¹⁶² In turn, biomimetic structural colours, which result from the physical interaction of light with nanostructures, have found application in the biomedical field. For example, hydrogels present distinct structural colours upon swelling or shrinking since a change in photonic band gap occurs.²⁴⁶ This has been applied in multiplex assay based on stomatocyte-mimetic photonic crystal (PhC) colour barcodes. Stomatocyte morphology was achieved by quick solvent extraction and self-assembling of monodispersed silica nanoparticles in aqueous droplets. This highly ordered structure was replicated using a hydrogel with suspended ferric oxide nanoparticles and the cavity was filled with platinum nanoparticles. Such micromotors could hence be driven by magnetic force and, when exposed to hydrogen peroxide solution, catalytic bubbles. Barcodes rely on the characteristic reflection peaks originating from the photonic band gap. Hence, by using structural colour-barcode micromotors with characteristic reflection peaks at 458, 565 and 650 nm (blue, green and red) modified with three distinct probes, a simultaneous detection of three kinds of DNA was performed (Figure 6D).²⁴⁷

Taking advantage of geometry via surface patterning or using diverse building blocks has proven to be a useful tool in biosensor design, which paves the way for the development of

further strategies and their employment in non-clinical and clinical research.

Conclusions

Recent advances in the tissue engineering and drug delivery fields have evidenced the impact of geometrical cues in controlling cell fate and tailoring drug release/cell targeting, respectively. Particularly in a 2D context, geometrical and topographical features have been highlighted as key moderators in controlling cell adhesion, morphology, and directing cell differentiation into specific lineages via their impact on mechanotransduction pathways. Topographical cues are associated with contact guidance and modulation of actomyosin contractility, while certain features have been shown to accelerate cell spreading. Consequently, differentiation is impacted by such cues and promising results have been evidenced for neurogenesis and osteogenesis applying grooves, pillars, and pits. Similarly, geometrical cues impact the generation of tension within the cell, which may be linked to alterations in cell proliferation, and cell fate towards adipogenic and osteogenic lineages, for instance.

Considering the more biomimetic 3D environment, microcarriers appear as attractive options for cell encapsulation and anchorage due to the possibility to easily modify and apply geometric and topographical features in combination with tuneable mechanical properties. Furthermore, microcarriers easily allow for a controlled cell spatial organisation for strategies featuring distinct cell populations, enabling “lock and key” assemblies. The application of these strategies has yielded promising reports in the literature, yet it is necessary to further study cell behaviour to pinpoint the mechanotransduction mechanisms in play in these 3D contexts. The role of topography in a 3D context has been greatly overlooked and warrants an advanced investigation, since results obtained in 2D do not easily transpose to what occurs in 3D. Similarly, microcarriers featuring distinct geometries have shown promising results for strategies aiming towards cell targeting, controlled drug delivery, and even production of biosensors, indicating that this strategy should be further pursued.

Recent advances in the field of biofabrication with new and improved techniques enable a growing control over feature morphology and intricacy of topographical details.²⁴⁸ With these advances, novel microparticle systems are expected to emerge for an efficient control over cell behaviour. Of course, these innovations bring even more possibilities to a table already full of options. Ultimately, *in silico* biomaterial design coupled with advanced fabrication techniques and high-throughput screening may be the way forward to test cellular response to such novel microcarriers.⁶⁰ In fact, high-throughput screening might evolve towards assessing the synergistic effect of both physical cues and material chemical of microcarriers.²⁴⁹

Author Contributions

Conceptualisation: I.M.B., C.R.C. and J.F.M.; Funding acquisition: C.R.C. and J.F.M.; Supervision: C.R.C. and J.F.M.; Writing – original draft: I.M.B.; Writing – review & editing: C.R.C. and J.F.M.

Conflicts of interest

There are no conflicts to declare.

Acknowledgements

I. M. Bjørge acknowledges financial support by the Portuguese Foundation for Science and Technology (FCT) with doctoral grant SFRH/BD/129224/2017. This work was supported by the European Research Council grant agreement ERC-2014-ADG-669858 for the project “ATLAS”. This work was financed by national funds (OE) through (FCT/MCTES) in the scope of the projects “TETRISUE”, reference PTDC/BTM-MAT/3201/2020 and “CIRCUS”, reference PTDC/BTM-MAT/31064/2017 also supported by the Programa Operacional Competitividade e Internacionalização, in the component FEDER (POCI-01-0145-FEDER-031064). This work was developed within the scope of the project CICECO-Aveiro Institute of Materials, UIDB/50011/2020 & UIDP/50011/2020, financed by national funds through the FCT/MEC and when appropriate co-financed by FEDER under the PT2020 Partnership Agreement.

References

- 1 C. M. Nelson and M. J. Bissell, *Annu. Rev. Cell Dev. Biol.*, 2006, **22**, 287–309.
- 2 S. R. Khetani and S. N. Bhatia, *Curr. Opin. Biotechnol.*, 2006, **17**, 524–531.
- 3 S. Dupont, L. Morsut, M. Aragona, E. Enzo, S. Giulitti, M. Cordenonsi, F. Zanconato, J. Le Digabel, M. Forcato, S. Bicciato, N. Elvassore and S. Piccolo, *Nature*, 2011, **474**, 179–183.
- 4 P. Fratzl and R. Weinkamer, *Prog. Mater. Sci.*, 2007, **52**, 1263–1334.
- 5 T. Dvir, B. P. Timko, D. S. Kohane and R. Langer, *Nat. Nanotechnol.*, 2011, **6**, 13–22.
- 6 T. L. Kline, M. Zamir and E. L. Ritman, *Cells. Tissues. Organs*, 2011, **194**, 431.
- 7 J. A. Brassard, M. Nikolaev, T. Hübscher, M. Hofer and M. P. Lutolf, *Nat. Mater.*, 2021, **20**, 22–29.
- 8 D. Lopes, C. Martins-Cruz, M. B. Oliveira and J. F. Mano, *Biomaterials*, 2018, **185**, 240–275.
- 9 T. N. Vo, F. K. Kasper and A. G. Mikos, *Adv. Drug Deliv. Rev.*, 2012, **64**, 1292–1309.
- 10 A. W. James, G. LaChaud, J. Shen, G. Asatrian, V. Nguyen, X. Zhang, K. Ting and C. Soo, *Tissue Eng. - Part B Rev.*, 2016, **22**, 284–297.
- 11 A. J. Engler, S. Sen, H. L. Sweeney and D. E. Discher, *Cell*, 2006, **126**, 677–689.
- 12 M. J. Dalby, N. Gadegaard and R. O. C. Oreffo, *Nat. Mater.*, 2014, **13**, 558–569.
- 13 A. Elosegui-Artola, R. Oria, Y. Chen, A. Kosmalska, C. Pérez-González, N. Castro, C. Zhu, X. Trepát and P. Roca-Cusachs, *Nat. Cell Biol.*, 2016, **18**, 540–548.
- 14 M. Bennett, M. Cantini, J. Reboud, J. M. Cooper, P. Roca-Cusachs and M. Salmeron-Sanchez, *Proc. Natl. Acad. Sci. U. S. A.*, 2018, **115**, 1192–1197.
- 15 W. Y. Wang, A. T. Pearson, M. L. Kutys, C. K. Choi, M. A. Wozniak, B. M. Baker and C. S. Chen, *APL Bioeng.*, 2018, **2**, 46107.
- 16 C. S. Chen, M. Mrksich, S. Huang, G. M. Whitesides and D. E. Ingber, *Science*, 1997, **276**, 1425–8.
- 17 L. Huang, A. M. E. Abdalla, L. Xiao and G. Yang, *Int. J. Mol. Sci.*, 2020, **21**, 1895.
- 18 Z. Zhou, W. Wu, J. Fang and J. Yin, *Int. Mater. Rev.*, 2021, **66**, 77–113.
- 19 M. D. Neto, M. B. Oliveira and J. F. Mano, *Trends Biotechnol.*, 2019, **37**, 1011–1028.
- 20 M. M. Maciel, T. R. Correia, M. Henriques and J. F. Mano, *Curr. Opin. Biotechnol.*, 2022, **73**, 276–281.
- 21 Z. Sun, S. S. Guo and R. Fässler, *J. Cell Biol.*, 2016, **215**, 445–456.
- 22 N. C. Gauthier and P. Roca-Cusachs, *Curr. Opin. Cell Biol.*, 2018, **50**, 20–26.
- 23 A. Elosegui-Artola, X. Trepát and P. Roca-Cusachs, *Trends Cell Biol.*, 2018, **28**, 356–367.
- 24 T. Mitchison and M. Kirschner, *Neuron*, 1988, **1**, 761–772.
- 25 C. E. Chan and D. J. Odde, *Science*, 2008, **322**, 1687–1691.
- 26 K. Hu, L. Ji, K. T. Applegate, G. Danuser and C. M. Waterman-Storer, *Science*, 2007, **315**, 111–115.
- 27 S. Kumar, I. Z. Maxwell, A. Heisterkamp, T. R. Polte, T. P. Lele, M. Salanga, E. Mazur and D. E. Ingber, *Biophys. J.*, 2006, **90**, 3762–3773.
- 28 M. Nikkhah, F. Edalat, S. Manoucheri and A. Khademhosseini, *Biomaterials*, 2012, **33**, 5230–5246.
- 29 M. Bao, J. Xie and W. T. S. Huck, *Adv. Sci.*, 2018, **5**, 1800448.
- 30 S. K. Mitra, D. A. Hanson and D. D. Schlaepfer, *Nat. Rev. Mol. Cell Biol.*, 2005, **6**, 56–68.
- 31 X. D. Ren, W. B. Kiosses, D. J. Siegel, C. A. Otey, D. D. Schlaepfer and M. A. Schwartz, *J. Cell Sci.*, 2000, **113**, 3673–3678.
- 32 E. Cukierman, R. Pankov, D. R. Stevens and K. M. Yamada, *Science*, 2001, **294**, 1708–1712.
- 33 K. Kimura, M. Ito, M. Amano, K. Chihara, Y. Fukata, M. Nakafuku, B. Yamamori, J. Feng, T. Nakano, K. Okawa, A. Iwamatsu and K. Kaibuchi, *Science*, 1996, **273**, 245–248.
- 34 K. Sao, T. M. Jones, A. D. Doyle, D. Maity, G. Schevzov, Y. Chen, P. W. Gunning and R. J. Petrie, *Mol. Biol. Cell*, 2019, **30**, 1170–1181.
- 35 A. M. Pasapera, I. C. Schneider, E. Rericha, D. D. Schlaepfer and C. M. Waterman, *J. Cell Biol.*, 2010, **188**, 877–890.
- 36 X. Zhu and R. K. Assoian, *Mol. Biol. Cell*, 1995, **6**, 273–82.
- 37 A. E. Miller, P. Hu and T. H. Barker, *Adv. Healthc. Mater.*, 2020, 1901445.
- 38 Y. L. Han, P. Ronceray, G. Xu, A. Malandrino, R. D. Kamm, M. Lenz, C. P. Broedersz and M. Guo, *Proc. Natl. Acad. Sci. U. S. A.*, 2018, **115**, 4075–4080.

- 39 K. Bhadriraju, M. Yang, S. Alom Ruiz, D. Pirone, J. Tan and C. S. Chen, *Exp. Cell Res.*, 2007, **313**, 3616–23.
- 40 J. Folkman and A. Moscona, *Nature*, 1978, **273**, 345–349.
- 41 R. J. Petrie, H. Koo and K. M. Yamada, *Science*, 2014, **345**, 1062–1065.
- 42 A. D. Doyle, F. W. Wang, K. Matsumoto and K. M. Yamada, *J. Cell Biol.*, 2009, **184**, 481–490.
- 43 O. Chaudhuri, L. Gu, D. Klumpers, M. Darnell, S. A. Bencherif, J. C. Weaver, N. Huebsch, H. Lee, E. Lippens, G. N. Duda and D. J. Mooney, *Nat. Mater.*, 2016, **15**, 326–334.
- 44 G. Nardone, J. Oliver-De La Cruz, J. Vrbsky, C. Martini, J. Pribyl, P. Skládal, M. Pešl, G. Caluori, S. Pagliari, F. Martino, Z. Maceckova, M. Hajduch, A. Sanz-Garcia, N. M. Pugno, G. B. Stokin and G. Forte, *Nat. Commun.*, 2017, **8**, 15321.
- 45 J. C. Rose and L. De Laporte, *Adv. Healthc. Mater.*, 2018, **7**, 1701067.
- 46 S. R. Caliari, S. L. Vega, M. Kwon, E. M. Soulas and J. A. Burdick, *Biomaterials*, 2016, **103**, 314–323.
- 47 J. Swift, I. L. Ivanovska, A. Buxboim, T. Harada, P. C. D. P. Dingal, J. Pinter, J. D. Pajerowski, K. R. Spinler, J.-W. Shin, M. Tewari, F. Rehfeldt, D. W. Speicher and D. E. Discher, *Science*, 2013, **341**, 1240104.
- 48 N. Huebsch, P. R. Arany, A. S. Mao, D. Shvartsman, O. A. Ali, S. A. Bencherif, J. Rivera-Feliciano and D. J. Mooney, *Nat. Mater.*, 2010, **9**, 518–26.
- 49 C. Loebel, R. L. Mauck and J. A. Burdick, *Nat. Mater.*, 2019, **18**, 883–891.
- 50 R. G. Wells, *Hepatology*, 2008, **47**, 1394–1400.
- 51 E. J. Semler, P. A. Lancin, A. Dasgupta and P. V. Moghe, *Biotechnol. Bioeng.*, 2005, **89**, 296–307.
- 52 S. F. B. Mennens, M. Bolomini-Vittori, J. Weiden, B. Joosten, A. Cambi and K. Van Den Dries, *Sci. Rep.*, 2017, **7**, 1–14.
- 53 Z. Li, Y. Gong, S. Sun, Y. Du, D. Lü, X. Liu and M. Long, *Biomaterials*, 2013, **34**, 7616–7625.
- 54 M. J. Dalby, M. O. Riehle, D. S. Sutherland, H. Agheli and A. S. G. Curtis, *Biomaterials*, 2004, **25**, 5415–5422.
- 55 M. J. Dalby, N. Gadegaard, R. Tare, A. Andar, M. O. Riehle, P. Herzyk, C. D. W. Wilkinson and R. O. C. Oreffo, *Nat. Mater.*, 2007, **6**, 997–1003.
- 56 Y. Hou, W. Xie, L. Yu, L. C. Camacho, C. Nie, M. Zhang, R. Haag and Q. Wei, *Small*, 2020, **16**, 1905422.
- 57 L. Pieuchot, J. Marteau, A. Guignandon, T. Dos Santos, I. Brigaud, P.-F. Chauvy, T. Cloatre, A. Ponche, T. Petithory, P. Rougerie, M. Vassaux, J.-L. Milan, N. Tusamda Wakhloo, A. Spangenberg, M. Bigerelle and K. Anselme, *Nat. Commun.*, 2018, **9**, 3995.
- 58 C.-S. Kim, J.-H. Kim, B. Kim, Y.-S. Park, H.-K. Kim, H. T. Tran, S. H. Kim, H. Jeon, S. Kim, J. H. Sim, H. M. Shin, G. Kim, Y. J. Baik, K.-J. Lee, H.-Y. Kim, T. J. Yun, Y. S. Kim and H.-R. Kim, *Adv. Funct. Mater.*, 2017, **27**, 1703569.
- 59 M. Hulsman, F. Hulshof, H. Unadkat, B. J. Papenburg, D. F. Stamatialis, R. Truckenmüller, C. van Blitterswijk, J. de Boer and M. J. T. Reinders, *Acta Biomater.*, 2015, **15**, 29–38.
- 60 F. Hulshof, B. Papenburg, A. Vasilevich, M. Hulsman, Y. Zhao, M. Levers, N. Fekete, M. De Boer, H. Yuan, S. Singh, N. Beijer, M. Bray, D. J. Logan, M. Reinders, A. E. Carpenter, C. Van Blitterswijk, D. Stamatialis and J. De Boer, *Biomaterials*, 2017, **137**, 49–60.
- 61 H. V Unadkat, M. Hulsman, K. Cornelissen, B. J. Papenburg, R. K. Truckenmüller, A. E. Carpenter, M. Wessling, G. F. Post, M. Uetz, M. J. T. Reinders, D. Stamatialis, C. A. van Blitterswijk and J. de Boer, *Proc. Natl. Acad. Sci. U. S. A.*, 2011, **108**, 16565–70.
- 62 E. T. den Braber, J. E. de Ruijter, L. A. Ginsel, A. F. von Recum and J. A. Jansen, *Biomaterials*, 1996, **17**, 2037–2044.
- 63 H. T. H. Au, I. Cheng, M. F. Chowdhury and M. Radisic, *Biomaterials*, 2007, **28**, 4277–4293.
- 64 E. Lamers, X. Frank Walboomers, M. Domanski, J. te Riet, F. C. M. J. M. van Delft, R. Luttge, L. A. J. A. Winnubst, H. J. G. E. Gardeniers and J. A. Jansen, *Biomaterials*, 2010, **31**, 3307–3316.
- 65 H. Moon, C. V. M. Cremmel, A. Kulpa, N. A. F. Jaeger, R. Kappelhoff, C. M. Overall, J. D. Waterfield and D. M. Brunette, *J. Biomed. Mater. Res. Part A*, 2016, **104**, 2243–2254.
- 66 M. D. Cabezas, B. Meckes, C. A. Mirkin and M. Mrksich, *ACS Nano*, 2019, **13**, 11144–11152.
- 67 S. A. Ruiz and C. S. Chen, *Stem Cells*, 2008, **26**, 2921–7.
- 68 D. Kim and D. Wirtz, *FASEB J.*, 2013, **27**, 1351–1361.
- 69 W. A. Loesberg, J. te Riet, F. C. M. J. M. van Delft, P. Schön, C. G. Figdor, S. Speller, J. J. W. A. van Loon, X. F. Walboomers and J. A. Jansen, *Biomaterials*, 2007, **28**, 3944–3951.
- 70 L. E. McNamara, T. Sjöström, K. Seunarine, R. D. Meek, B. Su and M. J. Dalby, *J. Tissue Eng.*, 2014, **5**, 2041731414536177.
- 71 D. Franco, M. Klingauf, M. Bednarzik, M. Cecchini, V. Kurtcuoglu, J. Gobrecht, D. Poulikakos and A. Ferrari, *Soft Matter*, 2011, **7**, 7313.
- 72 B. K. K. Teo, S. T. Wong, C. K. Lim, T. Y. S. Kung, C. H. Yap, Y. Ramagopal, L. H. Romer and E. K. F. Yim, *ACS Nano*, 2013, **7**, 4785–4798.
- 73 A. I. Teixeira, G. A. Abrams, P. J. Bertics, C. J. Murphy and P. F. Nealey, *J. Cell Sci.*, 2003, **116**, 1881–92.
- 74 E. K. F. Yim, E. M. Darling, K. Kulangara, F. Guilak and K. W. Leong, *Biomaterials*, 2010, **31**, 1299–306.
- 75 I. M. Bjørge, M. Salmeron-Sanchez, C. R. Correia and J. F. Mano, *Small*, 2020, **16**, 2001975.
- 76 L. E. McNamara, R. Burchmore, M. O. Riehle, P. Herzyk, M. J. P. Biggs, C. D. W. Wilkinson, A. S. G. Curtis and M. J. Dalby, *Biomaterials*, 2012, **33**, 2835–2847.
- 77 J. Y. Lim, A. D. Dreiss, Z. Zhou, J. C. Hansen, C. A. Siedlecki, R. W. Hengstebeck, J. Cheng, N. Winograd and H. J. Donahue, *Biomaterials*, 2007, **28**, 1787–1797.
- 78 S. J. Lee and S. Yang, *Rev. Sci. Instrum.*, 2012, **83**, 094302.
- 79 B. Sun, K. Xie, T.-H. Chen and R. H. W. Lam, *RSC Adv.*, 2017, **7**, 6788–6794.
- 80 K. Yang, K. Jung, E. Ko, J. Kim, K. I. Park, J. Kim and S.-W. Cho, *ACS Appl. Mater. Interfaces*, 2013, **5**, 10529–10540.
- 81 K. Yang, H. Jung, H.-R. Lee, J. S. Lee, S. R. Kim, K. Y. Song, E. Cheong, J. Bang, S. G. Im and S.-W. Cho, *ACS Nano*, 2014, **8**, 7809–7822.

- 82 S. Ankam, C. K. Lim and E. K. F. Yim, *Biomaterials*, 2015, **47**, 20–28.
- 83 G. Abagnale, M. Steger, V. H. Nguyen, N. Hersch, A. Sechi, S. Joussen, B. Denecke, R. Merkel, B. Hoffmann, A. Dreser, U. Schnakenberg, A. Gillner and W. Wagner, *Biomaterials*, 2015, **61**, 316–326.
- 84 M. J. Kim, B. Lee, K. Yang, J. Park, S. Jeon, S. H. Um, D. I. Kim, S. G. Im and S. W. Cho, *Biomaterials*, 2013, **34**, 7236–7246.
- 85 C. S. Chen, J. L. Alonso, E. Ostuni, G. M. Whitesides and D. E. Ingber, *Biochem. Biophys. Res. Commun.*, 2003, **307**, 355–361.
- 86 K. A. Kilian, B. Bugarija, B. T. Lahn and M. Mrksich, *Proc. Natl. Acad. Sci. U. S. A.*, 2010, **107**, 4872–7.
- 87 R. McBeath, D. M. Pirone, C. M. Nelson, K. Bhadriraju and C. S. Chen, *Dev. Cell*, 2004, **6**, 483–495.
- 88 T. C. von Erlach, S. Bertazzo, M. A. Wozniak, C.-M. Horejs, S. A. Maynard, S. Attwood, B. K. Robinson, H. Autebage, C. Kallepitis, A. del Río Hernández, C. S. Chen, S. Goldoni and M. M. Stevens, *Nat. Mater.*, 2018, **17**, 237–242.
- 89 J. H. Maduram, E. D. Goluch, H. Hu, C. Liu and M. Mrksich, *Cell Motil. Cytoskeleton*, 2008, **65**, 841–52.
- 90 T. Chen, A. Callan-Jones, E. Fedorov, A. Ravasio, A. Brugués, H. T. Ong, Y. Toyama, B. C. Low, X. Trepas, T. Shemesh, R. Voituriez and B. Ladoux, *Nat. Phys.*, 2019, **15**, 393–402.
- 91 M. Théry, A. Pépin, E. Dressaire, Y. Chen and M. Bornens, *Cell Motil. Cytoskeleton*, 2006, **63**, 341–355.
- 92 E. Kassianidou, D. Probst, J. Jäger, S. Lee, A.-L. Roguet, U. S. Schwarz and S. Kumar, *Cell Rep.*, 2019, **27**, 1897–1909.e4.
- 93 C. M. Nelson, R. P. Jean, J. L. Tan, W. F. Liu, N. J. Sniadecki, A. A. Spector and C. S. Chen, *Proc. Natl. Acad. Sci. U. S. A.*, 2005, **102**, 11594–11599.
- 94 W. R. Legant, A. Pathak, M. T. Yang, V. S. Deshpande, R. M. McMeeking and C. S. Chen, *Proc. Natl. Acad. Sci. U. S. A.*, 2009, **106**, 10097–10102.
- 95 P. Bose, J. Eyckmans, T. D. Nguyen, C. S. Chen and D. H. Reich, *ACS Biomater. Sci. Eng.*, 2019, **5**, 3843–3855.
- 96 D. E. Leckband and J. De Rooij, *Annu. Rev. Cell Dev. Biol.*, 2014, **30**, 291–315.
- 97 F. B. Hulshof, Y. Zhao, A. Vasilevich, N. R. M. Beijer, M. de Boer, B. J. Papenburg, C. van Blitterswijk, D. Stamatis and J. de Boer, *Acta Biomater.*, 2017, **62**, 188–198.
- 98 A. F. Adler, A. T. Speidel, N. Christoforou, K. Kolind, M. Foss and K. W. Leong, *Biomaterials*, 2011, **32**, 3611–3619.
- 99 S. Pettersson, J. Wetterö, P. Tengvall and G. Kratz, *Biomed. Mater.*, DOI:10.1088/1748-6041/6/6/065001.
- 100 C. A. Custódio, V. E. Santo, M. B. Oliveira, M. E. Gomes, R. L. Reis and J. F. Mano, *Adv. Funct. Mater.*, 2014, **24**, 1391–1400.
- 101 R. Yao, R. Zhang, F. Lin and J. Luan, *Biofabrication*, 2012, **4**, 045003.
- 102 K. J. Keville, E. J. Franses and J. J. Caruthers, *J. Colloid Interface Sci.*, 1991, **144**, 103–126.
- 103 C. Herrmann, M. B. Bannwarth, K. Landfester and D. Crespy, *Macromol. Chem. Phys.*, 2012, **213**, 829–838.
- 104 F. Friess, T. Roch, B. Seifert, A. Lendlein and C. Wischke, *Int. J. Pharm.*, 2019, **567**, 118461.
- 105 A. Sahari, M. A. Traore, B. E. Scharf and B. Behkam, *Biomed. Microdevices*, 2014, **16**, 717–725.
- 106 P. Zhang, L. Yang, Q. Li, S. Wu, S. Jia, Z. Li, Z. Zhang and L. Shi, *ACS Appl. Mater. Interfaces*, 2017, **9**, 7648–7657.
- 107 S. Orsi, E. Di Maio, S. Iannace and P. A. Netti, *Nano Res.*, 2014, **7**, 1018–1026.
- 108 J. A. Champion, Y. K. Katere and S. Mitragotri, *Proc. Natl. Acad. Sci.*, 2007, **104**, 11901–11904.
- 109 M. J. Heslinga, E. M. Mastria and O. Eniola-Adefeso, *J. Control. Release*, 2009, **138**, 235–242.
- 110 M. J. Heslinga, G. M. Willis, D. J. Sobczynski, A. J. Thompson and O. Eniola-Adefeso, *Colloids Surfaces B Biointerfaces*, 2014, **116**, 55–62.
- 111 Q. Fan, F. Qi, C. Miao, H. Yue, F. Gong, J. Wu, G. Ma and Z. Su, *Colloids Surfaces A Physicochem. Eng. Asp.*, 2016, **500**, 177–185.
- 112 I. M. Bjørge, A. M. S. Costa, A. S. Silva, J. P. O. Vidal, J. M. Nóbrega and J. F. Mano, *Soft Matter*, DOI:10.1039/c8sm00921j.
- 113 S. Wang, A. Bruning, O. Jeon, F. Long, E. Alsberg and C. K. Choi, *Biomicrofluidics*, 2018, **12**, 014106.
- 114 S. Wang, O. Jeon, P. G. Shankles, Y. Liu, E. Alsberg, S. T. Retterer, B. P. Lee and C. K. Choi, *Biomicrofluidics*, DOI:10.1063/1.4941339.
- 115 A. Leferink, D. Schipper, E. Arts, E. Vrij, N. Rivron, M. Karperien, K. Mittmann, C. van Blitterswijk, L. Moroni and R. Truckenmüller, *Adv. Mater.*, 2014, **26**, 2592–2599.
- 116 M. D. Tang, A. P. Golden and J. Tien, *J. Am. Chem. Soc.*, 2003, **125**, 12988–12989.
- 117 I. M. Bjørge, I. S. Choi, C. R. Correia and J. F. Mano, *Nanoscale*, 2019, **11**, 16214–16221.
- 118 D. Dendukuri, D. C. Pregibon, J. Collins, T. A. Hatton and P. S. Doyle, *Nat. Mater.*, 2006, **5**, 365–369.
- 119 P. Panda, S. Ali, E. Lo, B. G. Chung, T. A. Hatton, A. Khademhosseini and P. S. Doyle, *Lab Chip*, 2008, **8**, 1056–1061.
- 120 K. S. Paulsen and A. J. Chung, *Lab Chip*, 2016, **16**, 2987–2995.
- 121 J. Sun and N. M. Litchinitser, *ACS Nano*, 2018, **12**, 542–548.
- 122 Y. Xia and G. M. Whitesides, *Angew. Chemie Int. Ed.*, 1998, **37**, 550–575.
- 123 C. G. Williams, A. N. Malik, T. K. Kim, P. N. Manson and J. H. Elisseeff, *Biomaterials*, 2005, **26**, 1211–1218.
- 124 B. Liu, Y. Liu, A. K. Lewis and W. Shen, *Biomaterials*, 2010, **31**, 4918–4925.
- 125 Y. Zuo, X. Liu, D. Wei, J. Sun, W. Xiao, H. Zhao, L. Guo, Q. Wei, H. Fan and X. Zhang, *ACS Appl. Mater. Interfaces*, 2015, **7**, 10386–10394.
- 126 K. Cho, H. J. Lee, S. W. Han, J. H. Min, H. Park and W.-G. Koh, *Angew. Chemie Int. Ed.*, 2015, **54**, 11511–11515.
- 127 G. M. Whitesides, E. Ostuni, S. Takayama, X. Jiang and D. E. Ingber, *Annu. Rev. Biomed. Eng.*, 2001, **3**, 335–373.
- 128 J. Yeh, Y. Ling, J. M. Karp, J. Gantz, A. Chandawarkar, G. Eng, J. Blumling III, R. Langer and A. Khademhosseini, *Biomaterials*, 2006, **27**, 5391–5398.
- 129 B. Xue, V. Kozlovskaya and E. Kharlampieva, *J. Mater. Chem. B*, 2017, **5**, 9–35.

- 130 J. Xu, D. H. C. Wong, J. D. Byrne, K. Chen, C. Bowerman and J. M. DeSimone, *Angew. Chemie Int. Ed.*, 2013, **52**, 6580–6589.
- 131 F. P. W. Melchels, J. Feijen and D. W. Grijpma, *Biomaterials*, 2010, **31**, 6121–6130.
- 132 J. Y. Kelly and J. M. DeSimone, *J. Am. Chem. Soc.*, 2008, **130**, 5438–5439.
- 133 R. A. Petros, P. A. Ropp and J. M. DeSimone, *J. Am. Chem. Soc.*, 2008, **130**, 5008–5009.
- 134 A. M. Leferink, M. P. Tibbe, E. G. B. M. Bossink, L. E. de Heus, H. van Vossen, A. van den Berg, L. Moroni and R. K. Truckenmüller, *Mater. Today Bio*, 2019, **4**, 100025.
- 135 C. Ma, C. Tian, L. Zhao and J. Wang, *Lab Chip*, 2016, **16**, 2609–2617.
- 136 P.-J. Huang, C.-K. Chou, C.-T. Chen, H. Yamaguchi, J. Qu, A. Muliana, M.-C. Hung and J. Kameoka, *Soft Robot.*, 2017, **4**, 390–399.
- 137 A. N. Broers, *Philos. Trans. R. Soc. A Math. Phys. Eng. Sci.*, 1995, **353**, 291–311.
- 138 J. Jiang, S. Zhang, Z. Qian, N. Qin, W. Song, L. Sun, Z. Zhou, Z. Shi, L. Chen, X. Li, Y. Mao, D. L. Kaplan, S. N. Gilbert Corder, X. Chen, M. Liu, F. G. Omenetto, X. Xia and T. H. Tao, *Adv. Mater.*, 2018, **30**, 1705919.
- 139 E. R. Ruskowitz and C. A. DeForest, *Nat. Rev. Mater.*, 2018, **3**, 17087.
- 140 A. K. Nguyen and R. J. Narayan, *Mater. Today*, 2017, **20**, 314–322.
- 141 K. Parkatzidis, M. Chatzinikolaïdou, M. Kaliva, A. Bakopoulou, M. Farsari and M. Vamvakaki, *ACS Biomater. Sci. Eng.*, 2019, **5**, 6161–6170.
- 142 Z. Zheng, H. Wang, J. Li, Q. Shi, J. Cui, T. Sun, Q. Huang and T. Fukuda, *ACS Appl. Mater. Interfaces*, 2019, **11**, 22950–22961.
- 143 Y. Liu, C. Wu, H. Lu, Y. Yang, W. Li and Y. Shen, *Biofabrication*, 2019, **11**, 035019.
- 144 Z. Liu, M. Takeuchi, M. Nakajima, T. Fukuda, Y. Hasegawa and Q. Huang, *IEEE Robot. Autom. Lett.*, 2016, **1**, 206–212.
- 145 Z. Liu, M. Takeuchi, M. Nakajima, Y. Hasegawa, Q. Huang and T. Fukuda, *Acta Biomater.*, 2016, **37**, 93–100.
- 146 Z. Liu, M. Takeuchi, M. Nakajima, C. Hu, Y. Hasegawa, Q. Huang and T. Fukuda, *Acta Biomater.*, 2017, **50**, 178–187.
- 147 G. M. Whitesides, *Nature*, 2006, **442**, 368–373.
- 148 S. E. Chung, W. Park, H. Park, K. Yu, N. Park and S. Kwon, *Appl. Phys. Lett.*, 2007, **91**, 041106.
- 149 K. S. Paulsen, Y. Deng and A. J. Chung, *Adv. Sci.*, 2018, **5**, 1800252.
- 150 S. M. Nam, K. Kim, I.-S. Kang, W. Park and W. Lee, *BioChip J.*, 2019, **13**, 226–235.
- 151 W. Yang, H. Yu, G. Li, Y. Wang and L. Liu, *Small*, 2017, **13**, 1602769.
- 152 W. Yang, S. Cai, Y. Chen, W. Liang, Y. Lai, H. Yu, Y. Wang and L. Liu, *Adv. Mater. Technol.*, 2020, 1900847.
- 153 S. H. Park, J. Kim, W.-E. Lee, D.-J. Byun and M. H. Kim, *Langmuir*, 2017, **33**, 2275–2282.
- 154 R. Li, X. Li, L. Liu, Z. Zhou, H. Tang and Q. Zhang, *Macromol. Rapid Commun.*, 2010, **31**, 1981–1986.
- 155 W. Zhang, G. Huang, K. Ng, Y. Ji, B. Gao, L. Huang, J. Zhou, T. J. Lub and F. Xu, *Biomater. Sci.*, 2018, **6**, 885–892.
- 156 A. I. Neto, K. Demir, A. A. Popova, M. B. Oliveira, J. F. Mano and P. A. Levkin, *Adv. Mater.*, 2016, **28**, 7613–7619.
- 157 M. D. Neto, A. Stoppa, M. A. Neto, F. J. Oliveira, M. C. Gomes, A. R. Boccaccini, P. A. Levkin, M. B. Oliveira and J. F. Mano, *Adv. Mater.*, 2021, **33**, 2007695.
- 158 Z. Wu, Y. Yu, M. Zou, Y. Liu, F. Bian and Y. Zhao, *Compos. Commun.*, 2018, **10**, 129–135.
- 159 L. Wang, M. Qiu, Q. Yang, Y. Li, G. Huang, M. Lin, T. J. Lu and F. Xu, *ACS Appl. Mater. Interfaces*, 2015, **7**, 11134–11140.
- 160 A. G. B. Castro, M. C. Lo Giudice, T. Vermonden, S. C. G. Leeuwenburgh, J. A. Jansen, J. J. P. van den Beucken and F. Yang, *ACS Biomater. Sci. Eng.*, 2016, **2**, 2099–2107.
- 161 B. Almeria, W. Deng, T. M. Fahmy and A. Gomez, *J. Colloid Interface Sci.*, 2010, **343**, 125–133.
- 162 S. Park, H. J. Lee and W.-G. Koh, *Sensors*, 2012, **12**, 8426–8436.
- 163 R. K. Pal, N. E. Kurland, C. Jiang, S. C. Kundu, N. Zhang and V. K. Yadavalli, *Eur. Polym. J.*, 2016, **85**, 421–430.
- 164 F. Xu, T. D. Finley, M. Turkyaydin, Y. Sung, U. A. Gurkan, A. S. Yavuz, R. O. Guldiken and U. Demirci, *Biomaterials*, 2011, **32**, 7847–7855.
- 165 B. Zamanian, M. Masaëli, J. W. Nichol, M. Khabiry, M. J. Hancock, H. Bae and A. Khademhosseini, *Small*, 2010, **6**, 937–944.
- 166 D. Choi, E. Jang, J. Park and W.-G. Koh, *Microfluid. Nanofluidics*, 2008, **5**, 703–710.
- 167 M. H. M. Oudshoorn, R. Penterman, R. Rissmann, J. A. Bouwstra, D. J. Broer and W. E. Hennink, *Langmuir*, 2007, **23**, 11819–11825.
- 168 J. Hong, Y. Shin, S. Kim, J. Lee and C. Cha, *Adv. Funct. Mater.*, 2019, **29**, 1808750.
- 169 D. Lee, A. C. Lee, S. Han, H. J. Bae, S. W. Song, Y. Jeong, D. Y. Oh, S. Cho, J. Kim, W. Park and S. Kwon, *Biomicrofluidics*, 2018, **12**, 031102.
- 170 U. Bozuyuk, O. Yasa, I. C. Yasa, H. Ceylan, S. Kizilel and M. Sitti, *ACS Nano*, 2018, **12**, 9617–9625.
- 171 H. Ceylan, I. C. Yasa, O. Yasa, A. F. Tabak, J. Giltinan and M. Sitti, *ACS Nano*, 2019, **13**, 3353–3362.
- 172 Y. Yu, J. Guo, Y. Wang, C. Shao, Y. Wang and Y. Zhao, *ACS Appl. Mater. Interfaces*, 2020, **12**, 16097–16103.
- 173 J. C. Rose, D. B. Gehlen, T. Haraszti, J. Köhler, C. J. Licht and L. De Laporte, *Biomaterials*, 2018, **163**, 128–141.
- 174 A. P. McGuigan and M. V Sefton, *Proc. Natl. Acad. Sci. U. S. A.*, 2006, **103**, 11461–11466.
- 175 Y. He and K. Park, *Mol. Pharm.*, 2016, **13**, 2164–2171.
- 176 H. Qu, M. Yu, W. Du, L. Xu, W. Lyu and F. Shen, *Langmuir*, 2020, **36**, 585–590.
- 177 H. Tekin, T. Tsinman, J. G. Sanchez, B. J. Jones, G. Camci-Unal, J. W. Nichol, R. Langer and A. Khademhosseini, *J. Am. Chem. Soc.*, 2011, **133**, 12944–12947.
- 178 R. de Alteriis, R. Vecchione, C. Attanasio, M. De Gregorio, M. Porzio, E. Battista and P. A. Netti, *Sci. Rep.*, 2015, **5**, 12634.
- 179 S. E. A. Gratton, P. A. Ropp, P. D. Pohlhaus, J. C. Luft, V. J. Madden, M. E. Napier and J. M. DeSimone, *Proc. Natl.*

- Acad. Sci.*, 2008, **105**, 11613–11618.
- 180 N. Abbasi, M. Navi, J. K. Nunes and S. S. H. Tsai, *Soft Matter*, 2019, **15**, 3301–3306.
- 181 Zhihong Nie, Shengqing Xu, Minseok Seo, P. C. Lewis and E. Kumacheva, *JACS*, 2005, **127**, 8058–8063.
- 182 T. Nisisako, T. Ando and T. Hatsuzawa, *Small*, 2014, **10**, 5116–5125.
- 183 T. Nisisako and T. Hatsuzawa, *Microfluid. Nanofluidics*, 2010, **9**, 427–437.
- 184 Y. Hu, G. Azadi and A. M. Ardekani, *Carbohydr. Polym.*, 2015, **120**, 38–45.
- 185 S. Xu, Z. Nie, M. Seo, P. Lewis, E. Kumacheva, H. A. Stone, P. Garstecki, D. B. Weibel, I. Gitlin and G. M. Whitesides, *Angew. Chemie Int. Ed.*, 2005, **44**, 724–728.
- 186 Q.-W. Cai, X.-J. Ju, C. Chen, Y. Faraj, Z.-H. Jia, J.-Q. Hu, R. Xie, W. Wang, Z. Liu and L.-Y. Chu, *Chem. Eng. J.*, 2019, **370**, 925–937.
- 187 Z. Kang, T. Kong, L. Lei, P. Zhu, X. Tian and L. Wang, *J. Micromechanics Microengineering*, 2016, **26**, 075011.
- 188 A. J. D. Krüger, O. Bakirman, L. P. B. Guerzoni, A. Jans, D. B. Gehlen, D. Rommel, T. Haraszti, A. J. C. Kuehne and L. De Laporte, *Adv. Mater.*, 2019, 1903668.
- 189 D. K. Hwang, D. Dendukuri and P. S. Doyle, *Lab Chip*, 2008, **8**, 1640–1647.
- 190 D. Baah, J. Tigner, K. Bean, N. Walker, B. Britton and T. Floyd-Smith, *Microfluid. Nanofluidics*, 2012, **12**, 657–662.
- 191 R. Haghgooei, M. Toner and P. S. Doyle, *Macromol. Rapid Commun.*, 2010, **31**, 128–134.
- 192 W. Park, S. Jang, T. W. Kim, J. Bae, T. I. Oh and E. A. Lee, *Macromol. Biosci.*, 2019, **19**, 1900136.
- 193 K. Choi, M. Salehizadeh, R. B. Da Silva, N. Hakimi, E. Diller and D. K. Hwang, *Soft Matter*, 2017, **13**, 7255–7263.
- 194 M. Li, D. Joung, B. Hughes, S. D. Waldman, J. A. Kozinski and D. K. Hwang, *Sci. Rep.*, 2016, **6**, 30463.
- 195 J. W. Nichol and A. Khademhosseini, *Soft Matter*, 2009, **5**, 1312–1319.
- 196 B. Guillotin and F. Guillemot, *Trends Biotechnol.*, 2011, **29**, 183–190.
- 197 J. Rouwkema, N. C. Rivron and C. A. van Blitterswijk, *Trends Biotechnol.*, 2008, **26**, 434–441.
- 198 V. M. Gaspar, P. Lavrador, J. Borges, M. B. Oliveira and J. F. Mano, *Adv. Mater.*, 2020, **32**, 1903975.
- 199 C. R. Correia, I. M. Bjørge, S. Nadine and J. F. Mano, *Adv. Healthc. Mater.*, 2021, **2002110**, 1–18.
- 200 C. R. Correia, R. L. Reis and J. F. Mano, *Adv. Healthc. Mater.*, 2018, **7**, 1701444.
- 201 C. C. Ahrens, Z. Dong and W. Li, *Acta Biomater.*, 2017, **62**, 64–81.
- 202 C. A. Custódio, M. T. Cerqueira, A. P. Marques, R. L. Reis and J. F. Mano, *Biomaterials*, 2015, **43**, 23–31.
- 203 S. Utech, R. Prodanovic, A. S. Mao, R. Ostafe, D. J. Mooney and D. A. Weitz, *Adv. Healthc. Mater.*, 2015, **4**, 1628–1633.
- 204 C. R. Correia, I. M. Bjørge, J. Zeng, M. Matsusaki and J. F. Mano, *Adv. Healthc. Mater.*, 2019, 1901221.
- 205 D. R. Griffin, W. M. Weaver, P. O. Scumpia, D. Di Carlo and T. Segura, *Nat. Mater.*, 2015, **14**, 737–744.
- 206 F. Lim and A. M. Sun, *Science*, 1980, **210**, 908–10.
- 207 B. V. Slaughter, S. S. Khurshid, O. Z. Fisher, A. Khademhosseini and N. A. Peppas, *Adv. Mater.*, 2009, **21**, 3307–3329.
- 208 A. S. Mao, J.-W. Shin, S. Utech, H. Wang, O. Uzun, W. Li, M. Cooper, Y. Hu, L. Zhang, D. A. Weitz and D. J. Mooney, *Nat. Mater.*, 2017, **16**, 236–243.
- 209 P. de Vos, M. M. Faas, B. Strand and R. Calafiore, *Biomaterials*, 2006, **27**, 5603–5617.
- 210 C. R. Correia, R. L. Reis and J. F. Mano, *Biomacromolecules*, 2013, **14**, 743–751.
- 211 F. Li, V. X. Truong, P. Fisch, C. Levinson, V. Glattauer, M. Zenobi-Wong, H. Thissen, J. S. Forsythe and J. E. Frith, *Acta Biomater.*, 2018, **77**, 48–62.
- 212 L. Riley, L. Schirmer and T. Segura, *Curr. Opin. Biotechnol.*, 2019, **60**, 1–8.
- 213 G. Y. Huang, L. H. Zhou, Q. C. Zhang, Y. M. Chen, W. Sun, F. Xu and T. J. Lu, *Biofabrication*, 2011, **3**, 012001.
- 214 A. L. Van Wezel, *Nature*, 1967, **216**, 64–65.
- 215 A. C. Lima, C. Alvarez-Lorenzo and J. F. Mano, *Adv. Healthc. Mater.*, 2016, **5**, 1687–1723.
- 216 C. A. Custódio, R. L. Reis and J. F. Mano, *Adv. Healthc. Mater.*, 2014, **3**, 797–810.
- 217 A. Sheikhi, J. de Rutte, R. Haghniaz, O. Akouissi, A. Sohrabi, D. Di Carlo and A. Khademhosseini, *Biomaterials*, 2019, **192**, 560–568.
- 218 R. Mahou, A. E. Vlahos, A. Shulman and M. V. Sefton, *ACS Biomater. Sci. Eng.*, 2018, **4**, 3704–3712.
- 219 M. A. Skylar-Scott, S. G. M. Uzel, L. L. Nam, J. H. Ahrens, R. L. Truby, S. Damaraju and J. A. Lewis, *Sci. Adv.*, 2019, **5**, eaaw2459.
- 220 Z. Wang, J. Xia, Y. Yan, A.-C. Tsai, Y. Li, T. Ma and J. Guan, *Acta Biomater.*, 2015, **11**, 80–87.
- 221 H. Onoe and S. Takeuchi, *Drug Discov. Today*, 2015, **20**, 236–246.
- 222 E. Kang, Y. Y. Choi, S.-K. Chae, J.-H. Moon, J.-Y. Chang and S.-H. Lee, *Adv. Mater.*, 2012, **24**, 4271–4277.
- 223 C. R. Correia, S. Gil, R. L. Reis and J. F. Mano, *Adv. Healthc. Mater.*, 2016, **5**, 1346–1355.
- 224 J. Kim, J. R. Staunton and K. Tanner, *Adv. Mater.*, 2016, **28**, 132–137.
- 225 C. D. Paul, A. Hruska, J. R. Staunton, H. A. Burr, K. M. Daly, J. Kim, N. Jiang and K. Tanner, *Biomaterials*, 2019, **197**, 101–118.
- 226 K. E. Kasza and J. A. Zallen, *Curr. Opin. Cell Biol.*, 2011, **23**, 30–8.
- 227 D. Wei, W. Xiao, J. Sun, M. Zhong, L. Guo, H. Fan and X. Zhang, *J. Mater. Chem. B*, 2015, **3**, 2753–2763.
- 228 R. E. Unger, E. Dohle and C. J. Kirkpatrick, *Adv. Drug Deliv. Rev.*, 2015, **94**, 116–125.
- 229 C. R. Correia, R. P. Pirraco, M. T. Cerqueira, A. P. Marques, R. L. Reis and J. F. Mano, *Sci. Rep.*, 2016, **6**, 21883.
- 230 T. Sun, Q. Shi, Q. Huang, H. Wang, X. Xiong, C. Hu and T. Fukuda, *Acta Biomater.*, 2018, **66**, 272–281.
- 231 R. G. Flemming, C. J. Murphy, G. A. Abrams, S. L. Goodman and P. F. Nealey, *Biomaterials*, 1999, **20**, 573–588.
- 232 M. J. Dalby, *Med. Eng. Phys.*, 2005, **27**, 730–742.
- 233 C. J. Bettinger, R. Langer and J. T. Borenstein, *Angew.*

- Chem. Int. Ed. Engl.*, 2009, **48**, 5406–15.
- 234 Z. Nie and E. Kumacheva, *Nat. Mater.*, 2008, **7**, 277–290.
- 235 Q. Xu, M. Hashimoto, T. T. Dang, T. Hoare, D. S. Kohane, G. M. Whitesides, R. Langer and D. G. Anderson, *Small*, 2009, **5**, 1575–1581.
- 236 J. A. Ko, H. J. Park, S. J. Hwang, J. B. Park and J. S. Lee, *Int. J. Pharm.*, 2002, **249**, 165–174.
- 237 Y.-Y. Yang, T.-S. Chung and N. Ping Ng, *Biomaterials*, 2001, **22**, 231–241.
- 238 A. C. Lima, W. Song, B. Blanco-Fernandez, C. Alvarez-Lorenzo and J. F. Mano, *Pharm. Res.*, 2011, **28**, 1294–1305.
- 239 J. Xie, W. J. Ng, L. Y. Lee and C.-H. Wang, *J. Colloid Interface Sci.*, 2008, **317**, 469–476.
- 240 J. Siepmann and F. Siepmann, *J. Control. Release*, 2012, **161**, 351–362.
- 241 R. Mo and Z. Gu, *Mater. Today*, 2016, **19**, 274–283.
- 242 X. Lin, Z. Wu, Y. Wu, M. Xuan and Q. He, *Adv. Mater.*, 2016, **28**, 1060–1072.
- 243 Z. Wu, J. Li, B. E. F. De Ávila, T. Li, W. Gao, Q. He, L. Zhang and J. Wang, *Adv. Funct. Mater.*, 2015, **25**, 7497–7501.
- 244 W. Xu, P. Yin and M. Dai, *Angew. Chemie - Int. Ed.*, 2018, **57**, 14075–14079.
- 245 L. Sun, F. Bian, Y. Wang, Y. Wang, X. Zhang and Y. Zhao, *Proc. Natl. Acad. Sci. U. S. A.*, 2020, **117**, 4527–4532.
- 246 F. Fu, L. Shang, Z. Chen, Y. Yu, Y. Zhao, F. Fanfan, S. Luoran, C. Zhuoyue, Y. Yunru and Z. Yuanjin, *Sci. Robot.*, 2018, **3**, eaar8580.
- 247 L. Cai, H. Wang, Y. Yu, F. Bian, Y. Wang, K. Shi, F. Ye and Y. Zhao, *Natl. Sci. Rev.*, 2020, **7**, 644–651.
- 248 W. S. Harley, C. C. Li, J. Toombs, C. D. O’Connell, H. K. Taylor, D. E. Heath and D. J. Collins, *Bioprinting*, 2021, **23**, e00147.
- 249 L. Burroughs, M. H. Amer, M. Vassey, B. Koch, G. P. Figueredo, B. Mukonoweshuro, P. Mikulskis, A. Vasilevich, S. Vermeulen, I. L. Dryden, D. A. Winkler, A. M. Ghaemmaghami, F. R. A. J. Rose, J. de Boer and M. R. Alexander, *Biomaterials*, 2021, **271**, 120740.
- 250 F. Alisafaei, D. S. Jokhun, G. V. Shivashankar and V. B. Shenoy, *Proc. Natl. Acad. Sci. U. S. A.*, 2019, **116**, 13200–13209.